

## INVITED PAPER

# **RADIOCHEMICAL STUDY ON PHOTONUCLEAR REACTION MECHANISM AT INTERMEDIATE ENERGIES UPTO 1.2 GeV**

KOH SAKAMOTO

Kanazawa University, 302, 1-chome, Gosho-machi, Kanazawa, 920-0813, Japan

(Received May 28, 2010 and accepted June 01, 2010)

---

An account is given on radiochemical investigations on photonuclear reactions on target nuclei ranging from  ${}^7\text{Li}$  to  ${}^{209}\text{Bi}$  at intermediate energies up to 1.2 GeV, with use of bremsstrahlung beams of its maximum end-point energies of  $E_0 = 30\text{--}1200$  MeV with small steps of  $E_0$ , by the author's group since 1980s. The investigation covers the yield measurements of spallation, fragmentation, fission of the preactinides,  ${}^{197}\text{Au}$  and  ${}^{209}\text{Bi}$ , and photopion reactions, systematically performed with respect to photon energy ( $E_0$  and/or  $k$ ) target mass ( $A_t$ ) and/or target composition ( $N/Z$ )<sub>t</sub>, product mass ( $A$ ) and product composition ( $N/Z$ ). The analyses of the thousands of yield data obtained with aids of intensive chemical processings have yielded valuable insights into the reaction mechanism, *i.e.* characteristics of  $\Delta$ -resonance and strong effects of nuclear medium. In addition, a simple recoil experiment resulted valuable kinematic information regarding to the reaction steps. All of the results have updatedly used to test Monte Carlo calculations based on the photon-induced intranuclear cascade and evaporation analysis (PICA) code and its improved versions and the degrees of the validity of the codes have been demonstrated. New implications for the nuclear structure and reaction mechanism have been discussed by referring to the nuclear models on which the calculations are based.

**Keywords:** Photospallation, Photofragmentation, Photofission, Photopion reaction, Targets of  ${}^7\text{Li}$ - ${}^{209}\text{Bi}$ , Bremsstrahlung of 30-1200 MeV

---

### 1. Introduction

This paper is an account of our work on the title subject awarded by the 2009 Japan Society of Radiochemical and Nuclear Sciences, under the title of the Kimura prize in the honour of Late Professor Kenjiro Kimura (1896 – 1988), who was the founder of nuclear and radiochemistry in Japan.

Photonuclear reactions at intermediate energies have not been well documented in the standard nuclear and radiochemistry text books due to lack of the comprehensive experimental study before ours. It is now known that energetic photons are resonantly absorbed by atomic nuclei, *i.e.* (i) excitation to specific discrete excited levels of light- and medium-weight nuclei in an energy region of some keV – MeV, (ii) giant dipole resonance (GDR, resonance to dipole oscillation of a nucleus as a whole) around 20 MeV, (iii) quasi-deuteron resonance (QDR, resonance to dipole oscillation of proton and neutron pair inside a nucleus) at 30 to

140 MeV and (iv) At photon energies above pion threshold (140 MeV), an excited nucleon ( $\Delta$  isobar) is expected to be produced by the (3,3) resonance interaction,  $P_{33}$  (1232), of an incident photon with a single nucleon inside the target nucleus. The isobar decays immediately ( $10^{-24}$  sec) into a stable nucleon and a pion, and either or both particles produced in these initial processes would usually develop a cascade-evaporation process in the same nucleus, resulting in a multiple nucleon emission (spallation) and/or fission in case of heavy nuclei. The pion would give excitation energy of 140 MeV when its absorption occurs in the cascade process. Emissions of light nuclear clusters with mass numbers of  $A < 40$  in high energy photonuclear reactions on medium to heavy-weight targets have also been observed, but their formation mechanism during the cascade-evaporation process had not been well-understood as in high energy hadron reactions. During the process in an early stage of the cascade, one or

---

\* Corresponding author : kohsakamoto@par.odn.ne.jp

both of the particles may escape from the nucleus. The probability of the escape may depend on the location of photoabsorption by a nucleon and nuclear transparency for the associated particles. If the pion were emitted in a forward direction at a small angle, the residual nucleus would be left with an energy insufficient for developing the cascade-evaporation process. Especially, when photoabsorption occurs at the surface region of the target nucleus, the chance for an escape would be high and such simple reactions as  $(\gamma, n)$ ,  $(\gamma, p)$  and  $(\gamma, \pi^\pm)$  could result (surface reactions).

These simple reactions, especially on light nuclei have received considerable attention since 1950s in order to gain valuable basic information concerning photonuclear interactions and nuclear structure [1-3]. Photon sources for these experiments have been bremsstrahlung beams of continuous spectra ranging 0 to the maximum endpoint energies ( $E_0$ ) corresponding to the energies of electrons obtained from electron accelerators such as betatrons, electron linear accelerators (LINAC), and electron synchrotrons (ES). This continuous nature of bremsstrahlung beams makes the analyses of photonuclear reactions difficult. Most of the experimental studies were, therefore, directed to the double differential cross section measurements, *i.e.* the measurements of energies and angles of the emitted particles from the targets (inclusive measurements). Especially tagging systems allowing coincidence measurements of nuclear events with the accelerated electrons and bremsstrahlung photons, together with high resolution particle spectrometers, have been installed at most of high intensity and high energy electron accelerators for inclusive measurements during the late 1970s. However, it is difficult to identify the type of reactions responsible for the observed particles in the inclusive particle measurements, and there is an unavoidable restriction of the detection threshold ( $\sim 40$  MeV) of the particle spectrometers.

The activation method, first introduced by Hughes and March [4] who attempted to measure the residual nuclide of  $^{11}\text{B}(\gamma, \pi^-)^{11}\text{C}$  by observing its positron activity of 20 min half-life with use of the Glasgow 330 MeV ES as early as in 1957, was applied to many other heavier target nuclei ranging from  $^{27}\text{Al}$  to  $^{197}\text{Au}$  at the newly constructed accelerator sites mostly in USA, Russia (then USSR), Germany, Italy and Japan during 1960 – 1970. Studied were photospallation, photofission,

light nuclear cluster emission (fragmentation) alongwith the simple reactions mentioned above [5]. All of these pioneering experiments were performed by irradiation of bremsstrahlung beams of continuous spectra with  $E_0$  of 100 to 1000 MeV. Some were above 1000 MeV with uses of the 2.5 GeV ES at the University of Bonn, the 7.5 GeV ES at DESY, and the 5 GeV ES at the Yerevan Physics Institute, Armenia. The radioactivity measurements were performed mostly nondestructively with use of Ge(Li) detectors developed during this period. In an irradiation of medium- and heavy-nuclei, a huge variety of radionuclides produced mostly through spallation make an accurate measurement of those produced through other channels, such as photopion reactions, fission and fragmentation difficult and the reported results by different authors were often discrepant. The experimental studies on photonuclear reactions induced by bremsstrahlung beams had faded out in the late 1970s.

For the activation method a bremsstrahlung has still been a unique tool due to the absence of high energy monochromatic photon source with sufficiently high intensity. It has been expected to reveal the variation of the cross sections as a function of photon energy,  $k$ , (excitation function), when the irradiations are carried out at small steps of  $E_0$  to be sufficient enough for unfolding of the yield variations into the cross sections (see Sec. 6.1 below) as stated by Jonsson and Persson in their paper on  $^{127}\text{I}$ -photospallation in 1970 [6]. The activation method is useful for identifying the individual reactions unambiguously. Many radioisotopes decay to their isobaric daughter nuclides, which are observed as a sum of the primary product and its decay products (cumulative yield). Radiochemical methods can evaluate the respective contributions of the isobaric yields by changing the time of irradiation or that of chemical isolation.

The information obtained from the activation method is integral with respect to the energy and angle, and forgoes a detailed theoretical analysis of the final states involved. However, the complete picture concerning competitive reaction paths opened especially by  $\Delta$ -resonance such as photopion reactions  $(\gamma, \pi^x n)$  different in the number of neutrons emitted  $x$ , and the individual reactions leading to photospallation, photofragmentation and photofission can be clarified.

Under these situations by 1970s, we started to try the yield measurements of photonuclear reactions on a variety of targets ranging from  ${}^7\text{Li}$  to  ${}^{209}\text{Bi}$  at  $E_0 = 30 - 1200$  MeV in small  $E_0$  steps with the aid of intensive chemical separations of more than 200 recipes to systematize all types of residual radionuclides produced by photopion reaction [7-10], spallation [11-20], fragmentation [21, 22] and fission of pre-actinides,  ${}^{197}\text{Au}$  and  ${}^{209}\text{Bi}$  [23-25]. Empirical expressions for the reaction yields as well as for the parameters included in the expressions have been derived. A simple nuclear recoil experiment using thick-target thick-catcher method has been performed, in addition to the yield measurements, on 167 radionuclides formed in the photonuclear reactions of seven targets to obtain kinematic information and to deepen our understanding on reaction mechanism [17-20, 23-26]. All of the results have been discussed in conjunction with a theoretical calculation based on the photon-induced intranuclear cascade analysis code PICA) by Gabriel et al. [27, 28] and its improved versions by Fu [29] and Sato et al. [30,31]. Our experimental results have been used to test the validity of a new code by Mashnik et al. of Los Alamos Natl. Lab. [32].

In the following, I describe our experimental methods and the essential parts of the results of photopion reactions, spallation, fragmentation and fission separately, though all these processes are competitive. Some more detailed account has been published together with the literature quotations [5].

## 2. Experimental Procedures

Irradiations were performed using stacked targets with natural isotopic abundances (nat) in suitable chemical forms and sizes comprising of duplicated target disks and beam monitors. Electron-free collimated bremsstrahlung beams of  $E_0 = 250$  to 1200 MeV were supplied in air from the 1.3 GeV ES of the Institute for Nuclear Study (INS), the University of Tokyo (later The High Energy Accelerator Research Organization, KEK, at Tanashi). Uncollimated beams of  $E_0 = 30$  to 250 MeV were delivered from the 300 MeV Electron Linac of the Laboratory of Nuclear Science (LNS), Tohoku University. A series of irradiation of  $E_0 = 100$  to 250 MeV was performed in a water-cooled target holder with an electron beam being passed through an energy-compressing system to confine the electron energy to  $\pm 1\%$  at full width at half maximum. Irradiation of CsCl disks at 305 MeV

was tested in air with use of the 600 MeV Electron Linac at the Electrotechnical Laboratory (ETL). Bremsstrahlung was produced in a 0.5 mm-thick Pt converter both at LNS and ETL and in a 0.05 mm-thick Pt plate at INS. The size of the bremsstrahlung beam was about 10 mm in diameter at the target position both at INS and ETL, and about 5 mm in diameter at LNS. The beam intensity was monitored with a calibrated Wilson type thick chamber quantameter at INS, though the photon intensity used in the yield calculation for  $E_0 \geq 100$  MeV was obtained from the monitor reaction  ${}^{27}\text{Al}(\gamma, 2p\text{n}){}^{24}\text{Na}$  and those for  $E_0 = 30 - 75$  MeV was from  ${}^{197}\text{Au}(\gamma, n){}^{196}\text{Au}$  in aluminum and gold monitor foils., respectively, irradiated together with the targets. The yield data of the monitor reactions were experimentally examined by ourselves by referring to the reported values [33]. The average intensities in the series of irradiation were  $10^9 - 10^{10}$  equivalent quanta (eq.q.; see eqn.(6) below for definition) per second from INS ES and  $10^{12} - 10^{13}$  eq.q. per second from LNS linac.

After irradiation, chemical separation procedures of almost 200 recipes were applied to the target discs with use of proper carriers for  $\gamma$ -ray spectrometry and accelerator mass spectrometry, AMS, for  ${}^{10}\text{Be}$ , and without carrier for  $\alpha$ -spectrometry for polonium isotopes from  ${}^{209}\text{Bi}$  and for mercury isotopes from  ${}^{197}\text{Au}$  and for noble gas isotopes from  ${}^{41}\text{K}$ ,  ${}^{87}\text{Rb}$ ,  ${}^{127}\text{I}$ ,  ${}^{133}\text{Cs}$ , and  ${}^{139}\text{La}$ . The remaining irradiated targets were subjected to nondestructive  $\gamma$ -ray measurements. Radioactivity measurements were continued for more than one month in general to confirm the half-lives and no contribution from interferences.

## 3. Photospallation

### 3.1. Historical Aspect

Multiple nucleon emissions as expressed as  $(\gamma, xnyp)$ ,  $x$  and  $y$  being the numbers of neutrons and protons emitted, *i.e.* spallation, in high energy nuclear reactions are the most dominant competitive channel among others, and a broad spectrum of spallation residues is produced. The mechanism of hadron-induced spallation reactions has been explained by the intranuclear collision cascade and evaporation model by Serber [34] in 1947. The incident projectile initiates a knock-on cascade by the interaction with a nucleon inside the target nucleus, and a number of particles are ejected from the nucleus during the cascade. The residual nucleus is deexcited by the evaporation of

nucleons or nuclear clusters, and then the final product is formed. Systematic studies of photospallation seemed to be rather scanty in comparison with those by high energy hadrons (mostly protons) in the mid-1980s. The observed mass distribution of photospallation products appears very similar to the yield pattern of the hadron-induced spallation, in spite of the difference in the initial interactions; photospallation is initiated by purely electromagnetic interaction occurring deep inside the nucleus (volume interaction), while the hadron reaction is strong interaction induced by hadron incidence from the outside of the nucleus. It was of interest for us to confirm why the yield distributions are not affected by the difference of the initial interactions between photons and hadrons incident on the same target nucleus, though some earlier authors stated that the highly excited nucleus has lost its memory of formation.

A number of the previously reported results have been analysed with a five-parameter formula by Rudstam [35] who empirically derived it on the basis of the proton- and heavy ion-induced spallation data in a wide range of energy and mass. The proposed formula for charge distribution (CD) and mass distribution (MD) is

$$\sigma(Z, A) = \frac{\hat{\sigma} P R^{2/3} \exp\left[PA - R|Z - SA + TA^2|^{3/2}\right]}{1.79\{\exp(PA_t) - 1\}} \quad (1)$$

where  $\sigma(Z, A)$  is a formation cross section of a nuclide ( $Z, A$ ) produced from a target ( $Z_t, A_t$ ), and  $P, \hat{\sigma}, R, S$  and  $T$  are free parameters. The parameter  $P$  defines the slope of the mass yield curve,  $\hat{\sigma}$  the total inelastic cross section,  $R$  the width of CD and  $S$  and  $T$  the location of CD through the most probable charge  $Z_p = SA - TA^2$ .

Therefore, the parameters  $P$  and  $\hat{\sigma}$  define the shape of MD, the former the slope, *i.e.* indirect measure of excitation energy given to the target, and the latter the magnitude, and depend on both  $E_0$  and  $A_t$ . The parameter  $R$  is independent of the kind and energy of projectiles and depends on the product mass  $A$  and charge  $Z$ ;  $R = d' A^{-e'}$ ,  $d'$  and  $e'$  being constant. For the same reason as in the case of  $R$ , the peak position  $Z_p$  of CD depends on the proton and neutron separation energies and the Coulomb barrier and  $S$  and  $T$  can then be constant.

Owing to its success in the approximation of hadron-induced spallation with fairly good accuracy, Jonsson and Persson [6] tried to fit their data on  $^{127}\text{I}$ -photospallation at  $E_0 = 250 - 900$  MeV measured at steps of  $100 - 200$  MeV to the Rudstam formula in terms of the mean cross sections, *i.e.* the slope of linear array in spallation yield  $Y(E_0)$  vs.  $\ln E_0$  plots under the assumption of  $1/E_0$  variation for bremsstrahlung spectra. The significance of the different parameters was discussed by referring to those by the Rudstam's for particle-induced spallation. A number of the researchers also measured photospallation yields from various targets at higher  $E_0$ , and analyzed the data with the Rudstam formula and/or the Monte Carlo calculation (PICA). In the meantime, Jonsson and Lindgren [36] compiled and analysed the then available photo- and electro-spallation data with the five-parameter formula in terms of CDMD in 1973, and updated the systematics in 1977 [37]. They showed the capability of the CDMD-formula in predicting the yields and cross sections within a factor of about 2 with some exceptions of factors of upto 5, in broad energies and target masses with the new set of the parameter values. However, it was obvious that more precise parameters could not be obtained without more systematic measurements with respect to  $A_t, E_0$  and  $A$ .

Monte Carlo calculations on intranuclear cascades made by Metropolis et al. [38] in 1958 combined with the analytical treatment of the evaporation step given by Rudstam for high-energy protons [39] were utilized for calculations for photoreactions in the early days [6]. After 1970, the PICA code was occasionally tested also in terms of photospallation [40-42], too. A similar treatment was proposed by Barashenkov et al. [43] in 1974 for  $A \geq 27$  in photon energies of  $50$  MeV –  $1.3$  GeV, which gives higher mean excitation energy above  $k = 200$  MeV.

### 3.2. Similarity and Dissimilarity between Photospallation and Hadron Spallation

Under these historical situations, we first tried to observe the isotopic, isobaric and charge distributions by ourselves with an extensive radiochemical measurement of spallation from two mass regions; one of  $^{133}\text{Cs}$  and  $^{139}\text{La}$  [11], the other of  $^{\text{nat}}\text{Rb}$ ,  $^{\text{nat}}\text{Sr}$  and  $^{89}\text{Y}$  [12] at  $E_0 = 100$  and  $200$  MeV at LNS. The chemical separations of 5-7 elements were performed iteratively by changing the cooling time after irradiations to increase the number of

independent yields. The mass and charge distributions at the two  $E_0$  were examined with use of the Rudstam formula, and it was found that the spallation yields are governed by nuclear stability and the characteristic features previously reported are essentially correct.

The logarithmic slope of the mass yield curve,  $P$ , decreases linearly with an increase of the energy of proton and heavy ions up to  $\sim 2$  GeV and approaches a constant value in the higher energy region, the limiting regime, irrespective of incident particles [44-46] and the smaller slope has been suggested to be an indirect measure for higher deposition energy. On the other hand, the results of photospallations of  $^{51}\text{V}$  [40] and  $^{127}\text{I}$  [6] showed that the  $P$  values decrease with the increase of  $E_0$  up to 600 MeV and show a limiting above  $E_0 \geq 600$  MeV. This trend was confirmed also by us by extending  $E_0$  to 1000 MeV and was considered to be apparently different from those observed in the hadron spallation. Then the yields of 24 nuclides from photospallation of Cu were studied by nondestructive measurements at  $E_0 = 100 - 1000$  MeV in steps of 5 to 100 MeV at INS ES and compared directly with the results of proton and heavy ion spallation of Cu by Cumming et al. [44-46]. Figure 1 is the mass yield distributions for the products from Cu-photospallation at  $E_0 = 1000$  MeV (see also Fig. 4 for the data points obtained in later years). The comparison of the  $P$  values for Cu is shown in Figure 2, indicating that the  $P$  values of photospallation approach a constant value above 600 MeV, while those of hadron spallation attain the limiting regime at about 2 GeV as stated above and that the slope values of photospallation are larger than those of hadrons. It is plausible that these differences would partly be caused by the difference of the initial interaction between photon and hadron reactions. The width of the charge dispersion of Cu photospallation was found to be slightly narrower than that of proton spallation. The neutron-to-proton ratio of the most probable products,  $(N/Z)_p$ , in photospallation of Cu was estimated by  $Z_p = SA_m - TA_m^2$ , where the medium mass  $A_m = A_t - 1/P$  and  $1/P$  gives the average number of nucleons emitted, and found to be constant ( $1.148 \pm 0.003$  on average) in the  $E_0$  region of 100 – 1000 MeV. The results of  $(N/Z)_p$  obtained also from other photospallations showed a linear relationship with target  $(N/Z)_t$  as shown in Figure 3, but the slope of which is quite larger than that from proton- and  $\alpha$ - induced spallations of

targets with various values of  $(N/Z)_t$ . For the larger  $(N/Z)_t$ , the most probable product  $(N/Z)_p$  is shifted to the more neutron rich side in photospallation than in proton- and  $\alpha$ -spallation. Solid and dashed lines cross around  $(N/Z)_t = 1.2$  of Cu. This phenomenon is related to the average excitation energy of cascade residues produced in spallation process. At the end of the cascade process, the  $(N/Z)$  ratio of the cascade residues is approximately equal to  $(N/Z)_t$ . As the cascade residues are deexcited by evaporation, Coulomb barrier tends to suppress the emission of charged particles. The average excitation energy of the cascade residues in photospallation is lower than that in hadron spallation, as evidenced by the difference of the parameter  $P$ , and the emission of nucleon is relatively limited.

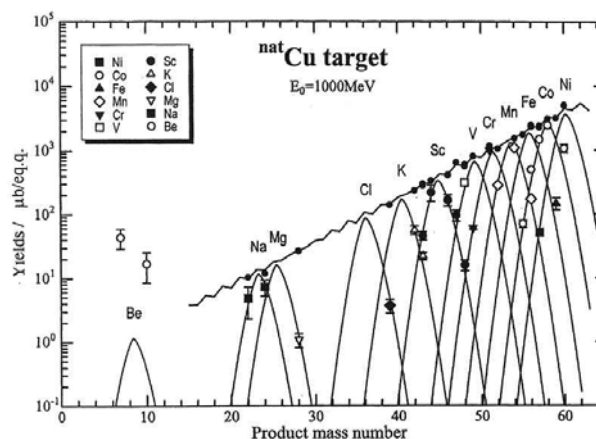


Figure 1. Yield distributions for products from  $^{nat}\text{Cu}(\gamma, xnp)$  reactions at  $E_0 = 1000$  MeV. Large symbols denote the measured yields obtained in our works [13]. Solid curves were from a nonlinear least-squares fit to the yield data. Small closed circles indicate the mass yields estimated by the Rudstam's formula (eqns. 1 and 2). Reprinted from Ref. 13. with permission from the American Physical Society, but revised to include the later data [47-49].

### 3.3. Systematics in Photospallation

A further extensive accumulation of photospallation yields was performed at  $E_0 = 30 - 1000$  MeV in steps of 100 MeV or less. The chosen targets were  $^{51}\text{V}$ ,  $^{59}\text{Co}$ ,  $^{89}\text{Y}$ ,  $^{127}\text{I}$ ,  $^{133}\text{Cs}$ ,  $^{139}\text{La}$ , and  $^{197}\text{Au}$ , and the number of the identified products were 22, 29, 31, 28, 44, 52, and 40, respectively. For most of the cumulative yields, corrections for the precursor-decays were performed by using the precursor yields obtained from the iterative least-squares fit of the Rudstam CDMD formula, the method of which was devised and reported [15].

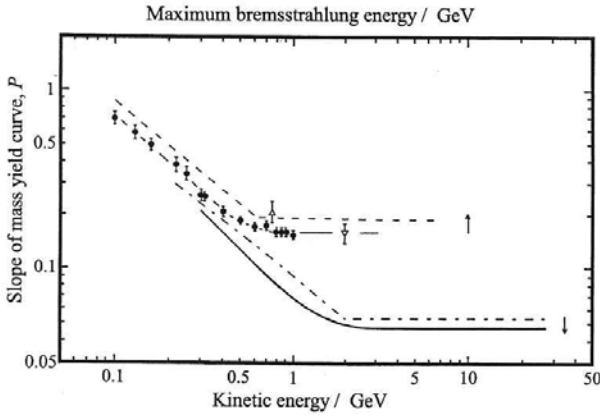


Figure 2. Logarismic slope of the mass yield curve ( $P$ ) as a function of  $E_0$  or  $E_h$ . Solid circles denote our work [13]. Open triangle denotes the value from Ref. 6, open inverted triangle denotes the data from N.M. Bachschi et al., Nucl. Phys. A264 (1976) 493. The thin solid curve is to guide eye for the solid circles. The dashed line was estimated for Cu target from the relations (3) in Ref. 37. The thick solid curve is for the slopes obtained by Cumming et al. [44-45] for Cu spallation induced by protons and heavy ions ( $^{14}\text{N}$ ,  $^{12}\text{C}$  and  $^{40}\text{Ar}$ ). Results for ( $\alpha$ -induced spallation of Cu by P.J.Karol, Phys. Rev. C10 (1974) 150 are also included. The dash-dotted line is for  $P$  values obtained by Rudstam [35]. (Reprinted from Ref. 13 with permission from the American Physical Society).

The individual yield data were carefully examined from the view points of self-consistency in the yield curves as a function of  $E_0$  and in the isotopic MD and CD. Then the expressions for the parameters in eqn. (1) by Jonsson and Lindgren [36,37] were revised ;

$$P = (134.8 \pm 27.1) A_t^{(-0.229 \pm 0.024)} E_0^{(-0.916 \pm 0.031)} \quad \text{at } 100 \leq E_0 \leq 600 \text{ MeV,}$$

$$P = (0.419 \pm 0.045) A_t^{(-0.229 \pm 0.024)} \quad \text{at } E_0 \geq 600 \text{ MeV}$$

$$\hat{\sigma} = [(-0.87 \pm 0.11) + (0.23 \pm 0.02) \ln E_0] A_t^{(1.03 \pm 0.03)} \text{ mb/eq.q.,} \quad (2)$$

$$R = (96.5 \pm 9.5) A^{(-0.95 \pm 0.05)},$$

$$S = 0.53 \pm 0.02, \text{ and } T = (6.5 \pm 3.5) \times 10^{-4} \text{ to give } Z_p = SA - TA^2$$

It should be noted that these parameter values were derived from the data on  $51 \leq A_t \leq 133$  and the products of ( $\gamma$ , xn) and ( $\gamma$ , pxn) reactions of  $x \geq 3 - 7$ . The degree of the fits of equation (2) to the

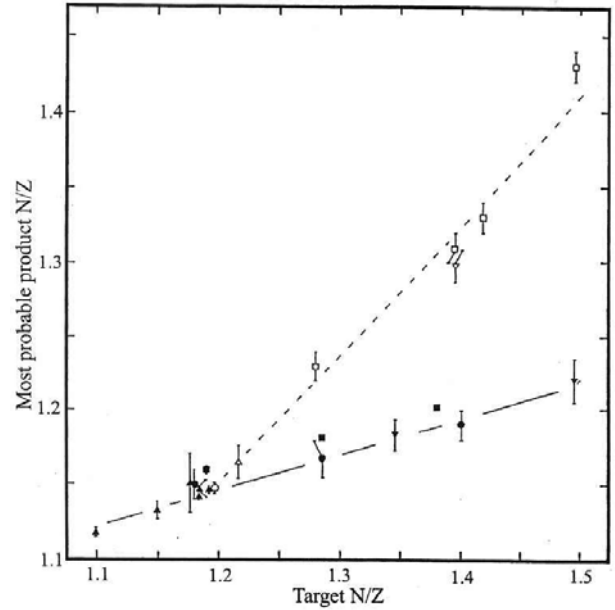


Figure 3. Most probable product  $(N/Z)_P$  as a function of target  $(N/Z)_t$ . Open symbols represent photon results and solid symbols proton- and ( $\alpha$ -results. Open circles denote our work [13], open triangle ( $\vee$  target) [37], open inverted triangle ( $\nabla$ ) [6], open squares ( $\Upsilon$ , I, Cs and Au ) by K. Sakamoto et al., Res. Rept. LNS, Tohoku Univ. 18 (1985) 290 solid circles ( $^{96}\text{Zr}$ ,  $^{96}\text{Mo}$  and  $^{96}\text{Ru}$ ) by N. T. Porile and L. B. Church, Phys. Rev. 133 (1964) B310, solid triangles (Ti, Fe, Co, Ni, Cu and Zn) by T. Asano et al., Phys. Rev. C28 (1983) 1718, solid inverted triangles (In and Au) by S. Kaufman, Phys. Rev. 129 (1963) 1866 solid squares (92, 96, 100Mo) by T. H. Ku and P. J. Karol, Phys. Rev. C16 (1977) 1984. The solid and dashed lines are to guide the eye. (Reprinted from Ref. 13 with permission from the American Physical Society).

experimental data is not satisfactory: 70 – 85 % of the data are within the quoted uncertainty and the remainings are within  $3\sigma$  at  $E_0 = 1000$  MeV. It seemed to be required for further refinement with the data for the products of larger  $\Delta A$  ( $= A_t - A$ ) from the heavier targets, but our later measurements indicated that the values in eqn. (2) are valid. Another empirical expression for the ( $\gamma$ , xn) yields of the near-by products to targets were derived :

$$\ln \sigma(Z_t, A) = ax + b$$

$$\text{with } a = (1.01 \pm 0.13) A^{(-6.61 \pm 0.64)} \text{ and } b = 6.78 \pm 0.21 \quad (3)$$

The slope  $a$  is independent of  $E_0$  of 300 – 1000 MeV, suggesting the contribution from low energy photons responsible for GDR and QDR [15].

The reproducibility of the Monte Carlo intranuclear cascade-evaporation calculation code by Gabriel and Alsmiller noted in Sec. 1 was examined with respect to the present photospallation data [16] in the early 1990s, by using the incident photon histories of  $(0.4 - 1.0) \times 10^6$  traced in each of 2 – 4  $E_0$ 's from 200 to 400 MeV for each target. It was concluded that the PICA code can be used to approximate photospallation yields and require improvements in many aspects. We have then extended our measurements of the yields of the products with larger  $\Delta A$  for the previously studied targets and new ones from  $^{27}\text{Al}$  to  $^{197}\text{Au}$  at  $E_0 = 60 - 1200$  MeV [20, 47-49]. The studied ranges of  $\Delta A$  were, for example, 190(61) for  $^{197}\text{Au}$ , (62) for  $^{\text{nat}}\text{Ag}$  and 82(50) for  $^{89}\text{Y}$ . The numbers in brackets are for spallation origin. Figure 4 shows some examples of MD. The PICA 3/GEM code [31] published in 2000, one of the updatedly improved versions of PICA code, was tested by tracing the particle histories of  $7 \times 10^7$ , and found to give a good agreement with the experiments though the smaller values for the yields for  $\Delta A \geq 40$  for  $^{59}\text{Co}$ ,  $\Delta A \geq 50$  for  $^{89}\text{Y}$  and  $\Delta A \geq 55$  for  $^{197}\text{Au}$  at  $E_0 = 400$  MeV appear, for example, as compared in Fig. 4. These discrepancies become smaller for heavier targets at higher  $E_0$ . Our systematic recoil experiments described below also indicate that the code reproduces well the kinematic properties for  $^{51}\text{V}$ ,  $^{\text{nat}}\text{Cu}$ ,  $^{93}\text{Nb}$  and  $^{\text{nat}}\text{Ag}$ , but under estimates the kinetic energies  $T$  of the residual nucleus in the heavy targets of  $^{181}\text{Ta}$  and  $^{197}\text{Au}$  (see Sec. 5).

## 4. Photofragmentation

### 4.1. Historical Aspect

Formation of light nuclei such as  $^7,^{10}\text{Be}$  and  $^{24}\text{Na}$  in high energy nuclear reactions on medium- to heavy-weight targets had been old questions regarding to reaction mechanisms. During 1950s, the radionuclide yields in the region of  $15 < A < 35$  were known to deviate largely from the expected spallation patterns in GeV-proton experiments. This was not explained by the cascade-evaporation model [51]. The term "fragmentation" has been coined for the formation process for these light nuclei in which the split-off of such a large piece of nuclear fragments from an excited nucleus during a nucleonic cascade is somehow supposed. Since

then, extensive studies have been continued radiochemically for proton-, neutron- and photon-induced reactions on a variety of targets, recently down to several tens of MeV [52]. An approximate feature of the cross section, mostly derived from proton reactions of 0.1 – several GeV, with respect to  $A_t$  and/or target asymmetry,  $[(N-Z)/A]_t$  has been obtained [53-55]. In photonuclear reactions, the apparent deviations of the yields of the light nuclei from the spallation systematics have been reported during the late 1960s to 1970s (see Figs. 1 and 4 for the concerned regions, as examples). "Photofission" was proposed for the formation mechanism of these light nuclei, along with "photofragmentation", though "spallation residue" mechanism can not be excluded in the reactions of the lighter targets closer to the products. We thought that the distinctions of the fragmentation and/or fission contributions from the total yields had to be somehow clarified experimentally before those complicated discussions.

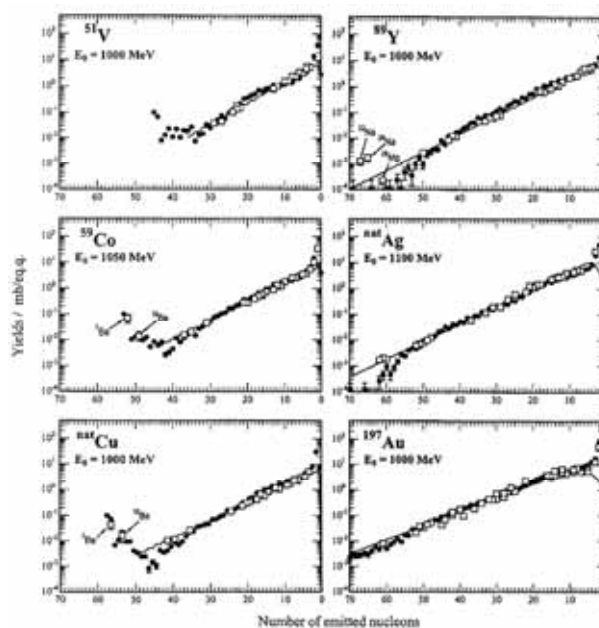


Figure 4. Measured mass yields from  $^{51}\text{V}$ ,  $^{59}\text{Co}$ ,  $^{\text{nat}}\text{Cu}$ ,  $^{89}\text{Y}$ ,  $^{\text{nat}}\text{Ag}$  and  $^{197}\text{Au}$  targets around  $E_0 = 1000$  MeV (open squares) together with those calculated with PICA3/GEM code (closed circles). Solid lines indicate the calculation with the Rudstam's formula (eqns. 1 and 2). (Constructed from Refs.13,14, 47 and 49 with permissions from the Japan Society of Nucl. Radiochem. Sciences and the Oldenbourg Wissenschaftsverlag).

#### 4.2. Systematic Study of Light Fragment Photoproductions

A series of the measurements of the isotopic pairs of  ${}^7,{}^{10}\text{Be}$  and  ${}^{22,24}\text{Na}$  up to  $E_0 = 1200$  MeV in steps of  $E_0 = 100$  MeV have then been performed on 23 targets ranging from  ${}^{\text{nat}}\text{B}$  to  ${}^{197}\text{Au}$ , with aids of AMS for  ${}^{10}\text{Be}$  and of a low-level counting technique for  ${}^{22}\text{Na}$  in addition to the standard gamma-ray spectrometry. The  ${}^{22}\text{Na}$  counting was performed at the Ogoya Underground Facility of the Low-Level Radioactivity Laboratory (LLRL) of Kanazawa University [56]. In addition, the photoreaction yields of  ${}^{28}\text{Mg}$ ,  ${}^{39}\text{Cl}$ ,  ${}^{43,44\text{m},44\text{g},46,47,48}\text{Sc}$ ,  ${}^{58}\text{Fe}$  and  ${}^{56,57,58,60}\text{Co}$  from the heavier targets were measured radiochemically to survey the contribution of fragmentation relative to spallation and/or fission in the mass yield distributions. The measured results were investigated in terms of  $E_0$ - and  $A_t$ -dependence of the yields and compared with those of proton reactions in the literature. A quantitative evaluation of the contribution of the fragmentation yields to the measured yields was obtained and a strong and clear effect of the target properties on the fragment formation was found.

##### 4.2.1. $E_0$ -dependence of Light fragment Yields

Figure 5 shows some typical examples of the yield variations as a function of  $E_0$ . The literature data from refs. [57-61] were included here. The arrows on the  $E_0$  axis indicate the Q values for spallation, *i.e.* ( $\gamma, xnyp$ ) reactions. The superscript and subscript of Q indicate the  $A_t$  and the numbers of the emitted neutron and proton, ( $x+y$ ), respectively. The yields increase steeply at low  $E_0$  and attain a plateau at  $E_0 = 400 - 500$  MeV for reaction with a small  $\Delta A$ , which is a typical feature of the (3,3) resonance (figures on left). In the reactions with larger  $\Delta A$ , *i.e.* the reactions on heavier targets, the yields increase slowly and reach a plateau at  $E_0 \geq 800$  MeV (figures on right). Those characteristics in the  $E_0$ -dependence are also observed in photospallation yields. The yield increase at  $E_0 \geq 600$  MeV appears to be ascribable to the medium effect in nuclei; broadening of excitation function [7, 8]. The reaction thresholds for the light nuclei from light targets are close to the Q-values for spallation, but those from heavier targets, *i.e.* with an increase of  $\Delta A$ , differ from the spallation Q, which were also observed in our earlier experiments [21]. This is a strong indication of contributions of fragmentation process, the thresholds of which is lower than the respective Q values for spallation.

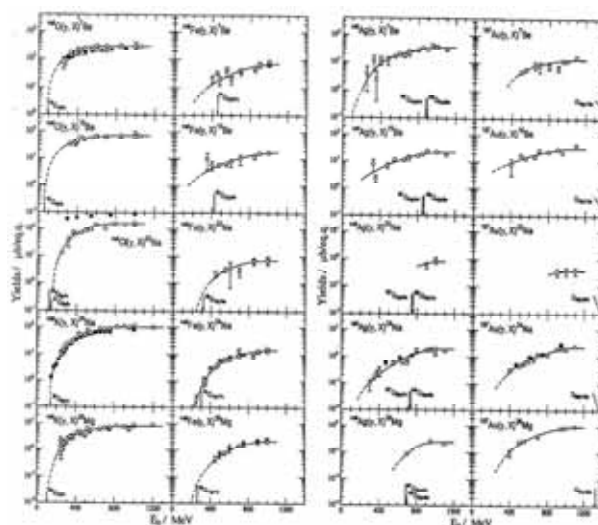


Figure 5. Typical examples of the measured yields of  ${}^7,{}^{10}\text{Be}$ ,  ${}^{22,24}\text{Na}$  and  ${}^{28}\text{Mg}$  from  ${}^{\text{nat}}\text{O}$ ,  ${}^{\text{nat}}\text{Cl}$ ,  ${}^{\text{nat}}\text{K}$ ,  ${}^{\text{nat}}\text{Fe}$ ,  ${}^{\text{nat}}\text{Ag}$ , and  ${}^{197}\text{Au}$  as a function of  $E_0$ . Open circles [22] and open squares [21] denote the values obtained in our works. Closed circles and closed squares indicate the data from Refs. [57- 61] respectively. Solid lines are drawn through the points to guide the eye. The arrows on the horizontal axis show the Q-values for the products as a spallation residue left after multiple nucleon emission. The superscript and subscript of Q indicate the mass number of the target and the number of the emitted nucleons in ( $\gamma, xnyp$ ) reaction, respectively, used for the Q-value calculation. (Reproduced from Ref. 22 with permission from the Oldenbourg Wissenschafts-verlag).

##### 4.2.2. $A_t$ -dependence of Light Fragment Yields.

We found that there exist two components in the  $A_t$ -dependence of the yields of  ${}^7\text{Be}$ ,  ${}^{10}\text{Be}$ ,  ${}^{22}\text{Na}$ ,  ${}^{24}\text{Na}$  and  ${}^{28}\text{Mg}$  as shown for  $E_0 = 1000$  MeV in Figure 6. The first component is a steep exponential decrease with an increase of  $A_t$  upto

40 – 80 for all of the five products, and the second is a slower exponential decrease of the  ${}^7\text{Be}$  and  ${}^{22}\text{Na}$  yields and a gradual increase of the  ${}^{10}\text{Be}$ ,  ${}^{24}\text{Na}$  and  ${}^{28}\text{Mg}$  yields at  $A_t \geq 40-80$ . The yields,  $Y(A_t)$  in unit of  $\mu\text{b}/\text{eq.q.}$  can be expressed as

$$Y(A_t) = a \cdot \exp(b \cdot A_t) + c \cdot \exp(d \cdot A_t) \quad (4)$$

The first component agrees with the values calculated by the Rudstam formula for spallation (eqn. 1) as marked by crosses in Fig. 6. The parameters a, b, c and d can be obtained by the

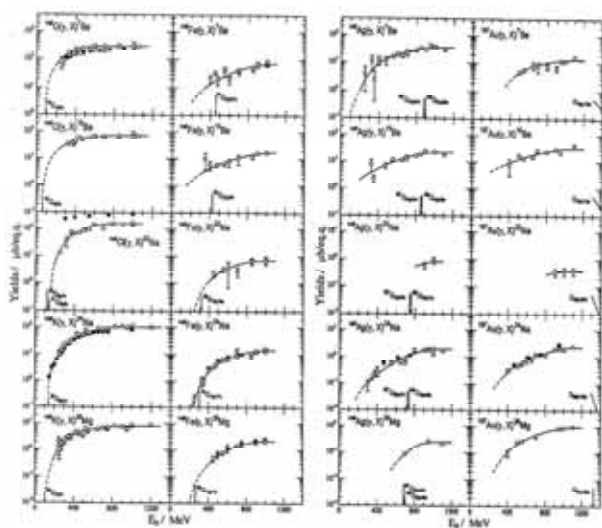


Figure 6. Yield variations of  ${}^7,{}^{10}\text{Be}$ ,  ${}^{22,24}\text{Na}$  and  ${}^{28}\text{Mg}$  at  $E_0 = 1000$  MeV as a function of target mass  $A_t$ . Open circles [22] and open squares [23] denote the values obtained in our works. Closed circles indicate the data from Refs. 58 and 59 and from V. di Napoli et al., J. Inorg. Nucl. Chem. **38** (1976)1. The data shown by closed squares are from Refs. 60 and 61. Crosses indicate the values calculated with the Rudstam's formula ( eqns.1 and 2) for spallation, (Reprinted from Ref. 22 with permission from the Oldenbourg Wissenschaftsverlag).

least squares fits to the two straight lines in each of subfigures of Fig. 6. The pure fragmentation yields corresponding to the second term of eqn. (4) of  ${}^7\text{Be}$  ( $N/Z = 0.75$ ) and  ${}^{22}\text{Na}$  ( $N/Z = 1.00$ ), which are deficient in neutron with respect to the  $\beta$ -stability valley, decrease exponentially with an increase of  $A_t$ , while the yields of neutron-rich  ${}^{10}\text{Be}$  ( $N/Z = 1.50$ ),  ${}^{24}\text{Na}$  ( $N/Z = 1.18$ ) and  ${}^{28}\text{Mg}$  ( $N/Z = 1.33$ ) increase with an increase of  $A_t$ . This fact means that the fragment production is largely dependent on target properties: the neutron-rich fragments are more probable from heavier target nuclei with higher  $(N/Z)_t$  (see Fig. 6) [22]. The preformation of nuclear clusters in an excited nuclei leading to fragmentation reflects the composition of the excited nuclei, and it was found that the fragment emissions occur after some neutrons from the excited targets. The reaction mechanism of  ${}^{24}\text{Na}$  was kinematically studied with use of catcher foil method, and found to be different from spallation nor fission [24, 26].

Comparison was made for the profiles of  $A_t$ -dependence of proton reaction cross sections and photoreaction yields for formation of the light

nuclei. Both of the profiles are energy-dependent, and the shape of the proton reactions at  $E_p = 600$  MeV is similar to those of photofragmentations at  $E_0 = 1000$  MeV. This is consistent with the fact that the effective photon energies in bremsstrahlung of  $E_0 = 1000$  MeV are 140 – 800 MeV for formation of these light nuclei. It was found that the proton data, especially for  ${}^{10}\text{Be}$  and  ${}^{28}\text{Mg}$ , are insufficient for further analysis.

#### 4.2.3. Perspectives

The PICA 3/GEM code indicated that the reproducibility of the fragment yields for  ${}^{7,10}\text{Be}$  is excellent as well as that of photospallation shown above, but those for the  ${}^{22,24}\text{Na}$  and  ${}^{28}\text{Mg}$  are still poor.

An increase of the sensitivity of the MALT-AMS in Tokyo has been allowing to measure both  ${}^{10}\text{Be}$  and  ${}^7\text{Be}$ , and one of my former students, Dr. H. Matsumura now at KEK, has successfully extended this type of study for 400 MeV-neutrons and alpha- particles-induced reactions. The Japan Society of Nucl. Radiochem. Society awarded him with the 2005 prize for Young Scientists for his achievement in the series of fragmentation study [62].

One of the breakthrough discoveries in the study on nuclear stability during the last decades was the spontaneous emission of  ${}^{14}\text{C}$  from  ${}^{223}\text{Ra}$  in 1984 [63], which has led an extensive development of cluster radioactivities, both experimentally and theoretically [64, 65]. This cold sub-barrier phenomenon has been tried to be understood by connecting to other phenomena such as  $\alpha$  radioactivity and spontaneous fission. A unified frame work to account for all these nuclear break-up phenomena that may differ in time sequence in the intranuclear process both in sub-barrier cold and highly excited hot regions of energy is expected from further clarifications of their individual aspects. Our efforts are believed to have given an important observational constraint to such developments.

## 5. Photofission

### 5.1. Historical Aspect

It was a natural consequence of photonuclear reaction study for us to pay our attention to fission products with mass range of  $A = 40 - 140$  from  ${}^{197}\text{Au}$  and  ${}^{209}\text{Bi}$ ; the outsides of fragmentation and spallation described above. The total photofission

yields or cross sections of  $^{197}\text{Au}$  and  $^{209}\text{Bi}$  as well as other pre-actinides and actinides at intermediate and high energies have extensively measured with ionization chambers and solid state detectors since 1950s. Reports of the CD and MD were not many, though the measurements are essential for understanding of fission mechanism.

Komar et al.[66] reported the symmetric MD with  $\text{FWHM}_{\text{MD}} = 40$  mass units (m.u.) for  $^{197}\text{Au}$  and 44 m.u. for  $^{209}\text{Bi}$  by coincident energy measurements of fission fragment pairs at  $E_0 = 1000$  MeV, assuming the mass of fissioning nucleus  $A_f = 194$  for the former and  $A_f = 205$  for the latter. Schröder et al. [67] measured the relative fission yields for 9 mass chains of  $A = 85 - 112$  from  $^{209}\text{Bi}$  at  $E_0 = 700$  MeV using a catcher foil technique, and reported a symmetric MD with the most probable mass  $A_p = 102.5$  m.u. and  $\text{FWHM}_{\text{MD}} = 22$  m.u. Di Napoli et al. [68] measured the yield of 11 fission products with  $A = 90 - 112$  from  $^{209}\text{Bi}$  at  $E_0 = 1000$  MeV radiochemically, and reported the MD with  $A_p = 101$  m.u. and  $\text{FWHM}_{\text{MD}} = 19$  m.u. On the other hand, Areskoug et al. measured the relative yields of 29 radionuclides from  $^{197}\text{Au}$  [69] and 43 radionuclides from  $^{209}\text{Bi}$  [70] at  $E_0 = 600$  MeV using the catcher foil technique, and analyzed the yields by a six-parameter CD and MD formula. The results were  $A_p = 92.6 \pm 0.6$  m.u. and  $\text{FWHM}_{\text{MD}} = 30.9 \pm 1.7$  m.u. for  $^{197}\text{Au}$  and  $A_p = 96.3 \pm 0.5$  m.u. and  $\text{FWHM}_{\text{MD}} = 34.8 \pm 0.7$  m.u. for  $^{209}\text{Bi}$ , and they mentioned that the larger widths of MD reported by Komar et al. were attributed to the higher photon energy investigated and that the values of  $A_p$  and  $\text{FWHM}_{\text{MD}}$  deduced by Schröder et al. and di Napoli et al. were not reliable due to the narrow mass ranges investigated.

## 5.2. Systematic Investigation of Photofission of $^{197}\text{Au}$ and $^{209}\text{Bi}$ .

For the fission study, irradiation was performed with a target stack of 5 – 50 sets of a Au foil of  $90 \text{ mg cm}^{-2}$  or a Bi plate of  $900 \text{ mg cm}^{-2}$ , both  $25 \times 25 \text{ mm}^2$  in size, sandwiched by one pair of  $3.5$  or  $7.0 \text{ mg cm}^{-2}$  thick Mylar foils of the same size, which collected the recoil nuclei in the forward and backward directions with respect to the beam direction. After irradiations, chemical separation of K, Sc, Fe, Ni, Zn, Ga, As, Rb, Sr, Y, Zr, Nb, Mo, Ag, Ba, and rare earth elements from Au and of Fe, Ga, As, Br, Sr, Y, Zr, Nb, Ag, I and Ba from Bi were employed for part of the targets to detect radionuclides with small yields. Gamma-ray assays

were performed for some selected targets and all of the forward and backward catchers from one target pile as well as the chemically separated samples.

Figure 7 shows the mass yield curves of the photofission of  $^{197}\text{Au}$  and  $^{209}\text{Bi}$  obtained by us at  $E_0 = 1000$  MeV [23, 25] alongwith photopion reactions, photospallation and photofragmentation for  $^{197}\text{Au}$ .

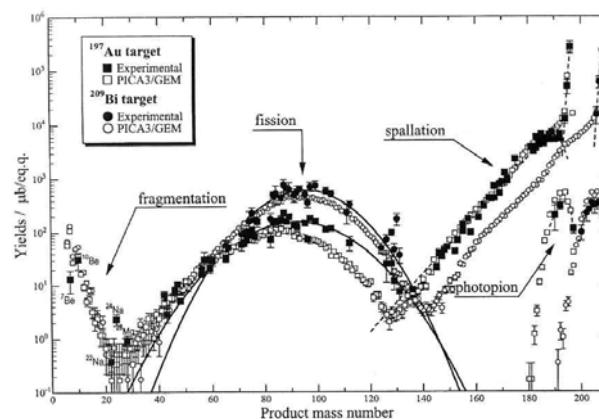


Figure 7. Experimental and calculated mass yields of photonuclear reactions of  $^{197}\text{Au}$  and  $^{209}\text{Bi}$  at  $E_0 = 1000$  MeV. The experimental yields from fission of  $^{197}\text{Au}$  and  $^{209}\text{Bi}$  are from Refs. 23 and 25. Those of photopion reactions on  $^{197}\text{Au}$  and  $^{209}\text{Bi}$  are from Ref. 10. Those of spallation of  $^{197}\text{Au}$  are from Refs. 14 and 47. Those of fragmentation from  $^{197}\text{Au}$  are from Ref. 22. The result of the PICA3/GEM are from Refs. 25, 47-49 and H. Haba et al., Proc. 43rd symp. on Radiochemistry, Oct. 13-15, Tsukuba, Japan. Suppl. To J. Nucl. Radiochem. Sci. Vol. 1, (1999) 3P18. (Constructed from the data in the cited refs. with permissions from the Japan Society of Nucl. Radiochem. Sciences and the Oldebourg Wissenschaftsverlag).

Here the reaction yields of 58 radionuclides as the fission products with the mass number  $A = 42 - 131$  from  $^{197}\text{Au}$  were measured at  $13E_0$ 's in the range from  $E_0 = 300$  to  $1100$  MeV in steps of 50 or 100 MeV, so shown in this figure is one example of  $13E_0$ 's. Thirty-six nuclides in the mass range of  $A = 46 - 131$  were identified both in the forward and backward catcher foils and 50 nuclides in the range of  $A = 42 - 131$  were in Au foils nondestructively and/or radiochemically. The recoil properties of 37 products in the mass range of  $24 \leq A \leq 131$  were also investigated alongwith the spallation results obtained for  $^{27}\text{Al}$ ,  $^{nat}\text{V}$ ,  $^{nat}\text{Cu}$ ,  $^{93}\text{Nb}$ ,  $^{nat}\text{Ag}$ ,  $^{nat}\text{Ag}$ ,  $^{nat}\text{Ta}$ ,  $^{197}\text{Au}$  and  $^{209}\text{Bi}$  [17-20] and compared with the literature data and the proton reactions [24]). For the  $^{209}\text{Bi}$  fission, the reaction yields of 63

radionuclides within  $A = 56 - 135$  were measured at six  $E_0$ 's in the range of  $E_0 = 450 - 1100$  MeV. The details are obtained in the original papers [23-25] and the summary is in an account [26] given by one of my former students, Dr. H. Haba now at RIKEN who received the 2001 Young Scientist Award from the Japan Society of Nucl. Radiochem. Society for this series of the recoil studies.

Also shown in this figure is the calculated result of the PICA3/GEM code for  $^{197}\text{Au}$  and  $^{209}\text{Bi}$  performed with particle histories of  $1 \times 10^9$  events for the former and  $5 \times 10^9$  events for the latter. The code is shown to reproduce the approximate features of MD and CD (not shown here) of  $^{197}\text{Au}$  fission, but the  $\text{FWHM}_{\text{CD}}$  of  $^{209}\text{Bi}$  fission is higher by 0.5 charge unit and the parameters  $R$  and  $S$  in the expression for the most probable charge,  $Z_p = R \cdot A + S$ , are discrepant from the experiment on  $^{209}\text{Bi}$ . The  $S$  value for  $^{197}\text{Au}$  is also higher by a factor of more than two compared with the experiment. The  $R$  value of  $(0.424 \pm 0.001)$  deduced for  $^{197}\text{Au}$  leads the number of prefission neutrons,  $\nu_{\text{pre}}$ , to be  $(11 \pm 1)$  through  $R = Z_t / (A_t - \nu_{\text{pre}})$  under the assumption of the unchanged charge distribution (UCD) hypothesis. The parameter  $S$  is a measure of the number of average post fission neutrons,  $\nu_{\text{post}}$  as  $S = Z_t - \nu_{\text{post}} / (A_t - \nu_{\text{pre}})$ . The  $S$  value of  $(0.7 \pm 0.1)$  deduced for  $^{197}\text{Au}$  leads the average  $\nu_{\text{post}}$  of  $(1.7 \pm 0.3)$ . The  $\nu_{\text{pre}}$  and  $\nu_{\text{post}}$  for  $^{209}\text{Bi}$  are  $(12 \pm 1)$  and  $(1.4 \pm 0.3)$ , respectively, which are comparable with those for  $^{197}\text{Au}$ . Therefore, the mass numbers of the fissioning nucleus  $A_f$  could be estimated to be 186 for  $^{197}\text{Au}$  and 197 for  $^{209}\text{Bi}$ . The most probable mass  $A_p$  of  $(92 \pm 1)$  m.u. of  $^{197}\text{Au}$  is 4 m.u. smaller than that of  $(96 \pm 1)$  m.u. of  $^{209}\text{Bi}$  and the  $\text{FWHM}_{\text{MD}}$  of  $(39 \pm 1)$  m.u. is larger by 6 m.u. than that of  $(33 \pm 3)$  m.u. The reported  $A_p$  and  $\text{FWHM}_{\text{MD}}$  described above are not consistent with ours except for those by Areskoug et al. The same is true for the charge distribution parameters  $\text{FWHM}_{\text{CD}}$ ,  $R$  and  $S$  for  $^{197}\text{Au}$  at  $E_0 = 600$  MeV. The discrepancies may be attributed to the smaller mass range analysed.

The total fission yields of  $^{197}\text{Au}$  and  $^{209}\text{Bi}$  in unit of mb/eq.q. were deduced from the mass yield curves as a function of  $E_0$ , and compared with literature data [23, 25] for the details). The total fission yields increase steeply by about three order of magnitude with increase of  $E_0$  from 100 MeV to

600 MeV and increase slightly above  $E_0 = 600$  MeV. Total fission yield of  $(10 \pm 1)$  mb/eq.q. for  $^{209}\text{Bi}$  at 1000 MeV is about three times higher than the value of  $(3.2 \pm 0.1)$  mb/eq.q. for  $^{197}\text{Au}$ . This difference is explained by a systematic trend of nuclear fissility,  $f$ , as a function of  $Z^2/A$ . i.e.  $f = \exp[0.87(Z^2/A - 35.83)]$  [71]. The calculated fission yields by the PICA3/GEM code give smaller values compared with the experiments for both  $^{197}\text{Au}$  and  $^{209}\text{Bi}$ , respectively. Since 1980s, total fission yields and/or cross sections have been intensively measured with glass or plastic track detectors or multiwire spark chamber in irradiations with quasi-monochromatic photon beams of energies up to 300 MeV, produced from in-flight positron annihilation at Mainz Linac, Laboratorio Esperienze Acceleratore Lineare Elettroni (LEALE) of Frascati ES, Italy, or from backward Compton scattering of laser light on electrons circulating in a storage ring ADONE facility of Frascati ES, Laser Electron Gamma Source (LEGS) facility of Brookhaven National Laboratory and of ROKK 1M and ROKK 2M of Budker Institute of Nuclear Physics, Novosibirsk, and the detailed structure of the excitation function of photofissions has getting clear. Those beams of  $10^5 - 10^6$  photons/sec are unfortunately too low in intensities for our types of radiochemical study.

### 5.3. Recoil Properties of Photospallation Products from Complex Nuclei and of Photofission Products from $^{197}\text{Au}$

From the fractions of each nuclide measured for  $^{27}\text{Al}$ ,  $^{\text{nat}}\text{V}$ ,  $^{\text{nat}}\text{Cu}$ ,  $^{93}\text{Nb}$ ,  $^{\text{nat}}\text{Ag}$ ,  $^{\text{nat}}\text{Ta}$  and  $^{197}\text{Au}$  in the forward and backward catcher foils, expressed as

$$F = N_F / (N_F + N_B + N_{\text{target}}) \text{ and}$$

$$B = N_B / (N_F + N_B + N_{\text{target}}),$$

$N$  being the number of atoms, the effective mean ranges  $\text{FW}$  and  $\text{BW}$  were obtained by multiplying the target thickness  $W$  in unit of  $\mu\text{g cm}^{-2}$  and found to be independent of  $E_0$  above 600 MeV. This is consistent with the  $E_0$ -dependence of the slope parameter  $P$  described in Sec. 3.2 above. Figure 8 shows the averaged values of  $\text{FW}$  and  $\text{BW}$  for  $^{\text{nat}}\text{Cu}$  (Fig. 8a) and  $^{197}\text{Au}$  (Fig. 8b) as a function of mass difference  $\Delta A$  between a product ( $A_p$ ) and a target ( $A_t$ ). The  $\text{FW}$  values are higher than the corresponding  $\text{BW}$ , and both increase in parallel with an increase of  $\Delta A$ .

Those increasing curves with  $\Delta A$  can be divided into two components: one is a steep increase for the  $(\gamma, xn)$  product by GDR and the other is a gentle increase for the  $(\gamma, xnyp)$ ,  $(x, y \geq 1)$  products mainly produced by  $\Delta$ -resonance. This finding is also consistent with the result of the CDMD analysis mentioned in Sec. 3.3. The forward-backward ratios F/B at  $E_0 \geq 600$  MeV was found to be independent of  $\Delta A$  as expected from the parallel changes of FW and BW. It is noted that the F/B ratios of proton spallations at  $E_p \leq 3$  GeV vary with  $\Delta A$  and decrease with an increase of  $E_p$ , but become  $E_p$ - and  $\Delta A$ -independent above 3 GeV.

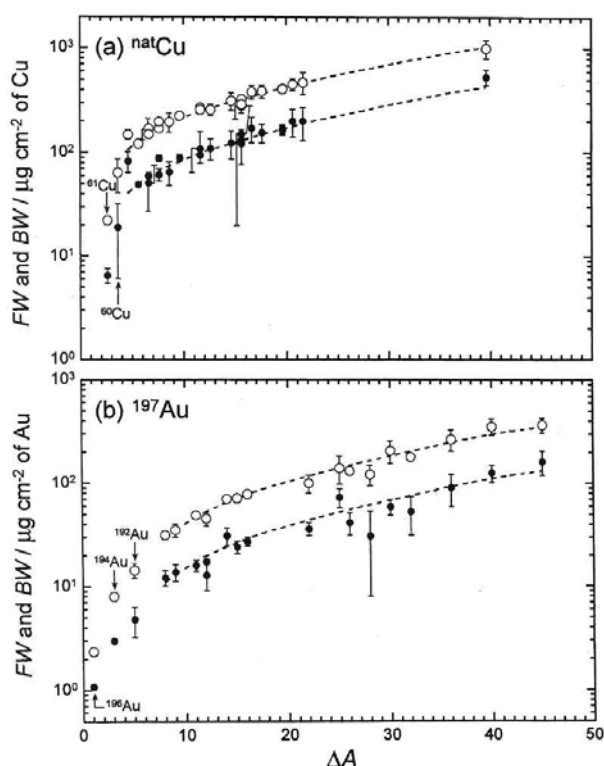


Figure 8. Averaged mean ranges FW (open symbols) and BW (closed symbols) at  $E_0 \geq 600$  MeV as a function of mass difference  $\Delta A (= A_t - A)$  for (a)  $^{nat}\text{Cu}$  and (b)  $^{197}\text{Au}$ . The dashed curves are to guide the eye. ( From Ref. 20 with permission from the Oldenbourg Wissenschaftsverlag ).

The measured recoil data were used to derive some recoil parameters by mean of the two-step vector velocity model developed for proton reactions by Winsberg [72]. According to this model, the observable velocity  $v_1$  of a recoiling nucleus is resolved into two velocity components,  $v$  and  $V$ , corresponding to the cascade step and the deexcitation or breakup step of the reaction,

respectively. The cascade component  $v$  is assumed to be parallel to the beam direction. The velocity  $V$  must be symmetric in the moving system and is assumed to be isotropic. If the range of a recoiling nucleus in the target material  $R_1$  can be related to its velocity by an expression of  $R_1 = Cv_1^N$ , where  $C$  and  $N$  are constants, and if  $v/V$  is small, the following relations can be derived:

$$FW = \frac{R_0}{4} \left\{ 1 + \frac{2(N+2)v}{3} \frac{v}{V} + \frac{(N+1)^2}{4} \left( \frac{v}{V} \right)^2 \right\} \quad (5)$$

$$BW = \frac{R_0}{4} \left\{ 1 - \frac{2(N+2)v}{3} \frac{v}{V} + \frac{(N+1)^2}{4} \left( \frac{v}{V} \right)^2 \right\}$$

The quantity  $R_0$  is the mean range in the target material corresponding to the recoil velocity  $V$ , so that  $R_0 = CV^N$ . The  $R_0$  and  $v/V$  are calculated from the measured FW and BW by eqn.(3) above. The calculated  $R_0$  can be converted to the kinetic energy  $T$  of the residual nucleus and the values of  $C$  and  $N$  by using the SRIM 2000 code developed by Ziegler et al. [73] for range-energy relation. The forward velocity  $v$  is calculated from the  $v/V$  and  $T$  values.

The mean ranges  $R_0$  in unit of  $\text{mg cm}^{-2}$  of target foils of spallation products at  $E_0 \geq 600$  MeV were found to be smoothly increasing functions of  $\Delta A$ , which are expressed as  $R_0 = a \cdot (A_t/\Delta A - 1)^{-b}$  where the parameters  $a$  and  $b$  can be obtained by the least-squares fittings and are a smooth function of atomic number of target  $Z_t$ . The forward velocity  $v$  is a good parameter to estimate the momentum transferred to an intermediate nucleus in the first cascade step and is related to the deposited excitation energy. On the other hand, the average recoil energy  $T$  imparted to a recoiling nucleus is a good parameter to investigate the second evaporation step of the reaction. The variations of  $v$  and  $T$  at  $E_0 \geq 600$  MeV as a function of  $\Delta A$  are shown by large open circles for  $^{nat}\text{Cu}$  as an example, in Figures 9a and 9b, respectively. The cascade velocity  $v$  increases linearly with an increase of  $\Delta A$ , indicating that the higher excitation energy is deposited on an intermediate nucleus to form a residual nucleus with a larger  $\Delta A$ . The kinetic energy  $T$  is also an increasing function of  $\Delta A$ , as explained by a random-walk theory [74]. Proton results available at various proton energies  $E_p$ , as shown in the inset of Fig. 9b [26] for the

quoted references in the inset), are compared. The  $v$  values at  $E_p \leq 3$  GeV (open symbols) are apparently higher than those of photoreactions and decrease with an increase of  $E_p$  up to 3 GeV and those at  $E_p > 3$  GeV (closed symbols) are almost the same as those of photoreactions. But all of the  $T$  values of the proton reactions are about the same as those of photoreactions, irrespective of  $E_p$ . These findings are also the same for other targets studied in our works and consistent with the limiting characters mentioned in Sec. 3.2. It is noted that  $T$  in proton reactions is independent of  $E_p$  and agrees with  $T$  in photoreactions. This fact implies that the mechanism of the second deexcitation step is very similar in both types of reactions.

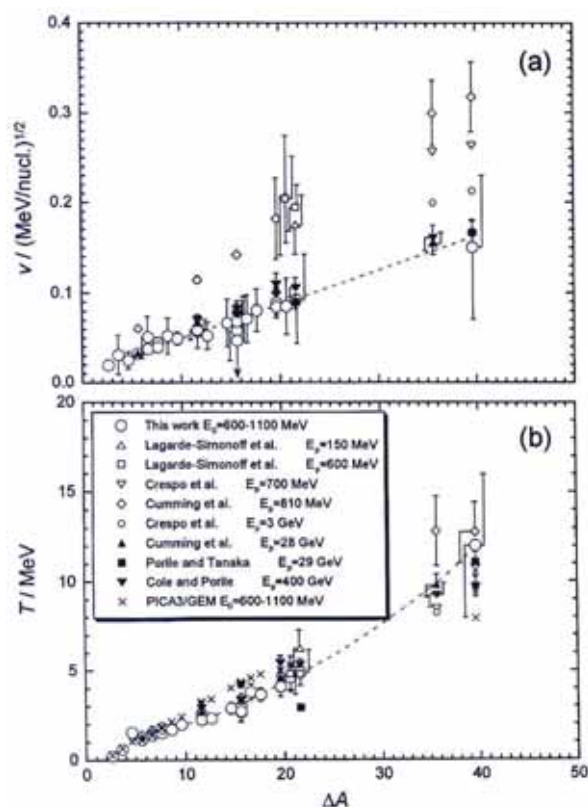


Figure 9. (a) Forward velocity  $v$  in the first step and (b) kinetic energy  $T$  in the second step as a function of  $\Delta A$  for  $^{nat}\text{Cu}$  (From Ref. 20 with permission from the Japan Society of Nucl. Radiochem. Society).

The reproducibility of  $T$  by the PICA3/GEM code was examined as exemplified by crosses in Fig. 7b. The calculated  $T$  was found to reproduce fairly well those for  $^{nat}\text{Cu}$  to  $^{nat}\text{Ag}$ , but to underestimate those for heavier targets of  $^{nat}\text{Ta}$  and  $^{197}\text{Au}$ . This discrepancy in the heavy targets is explained by

”nuclear medium effect”, as will also be shown below in Sec. 6.3.

Winsberg [74] suggested that  $\epsilon_s = T/(\Delta A/A_t)$ , which represents the average energy carried off by an evaporated nucleon, is a good parameter to systematize the second step, and found that  $\epsilon_s$  is independent of  $\Delta A/A_t$  and also of  $A_t$  for proton spallation. This idea was applied to our photoreactions. The  $\epsilon_s$  values of the  $(\gamma, xn)$  products increase with an increase of  $\Delta A/A_t$  and those of the  $(\gamma, xnyp)$  products are shown to be constant, as shown in Figure 10. The  $A_t$ -dependence of  $\epsilon_s$  of both the photon and proton

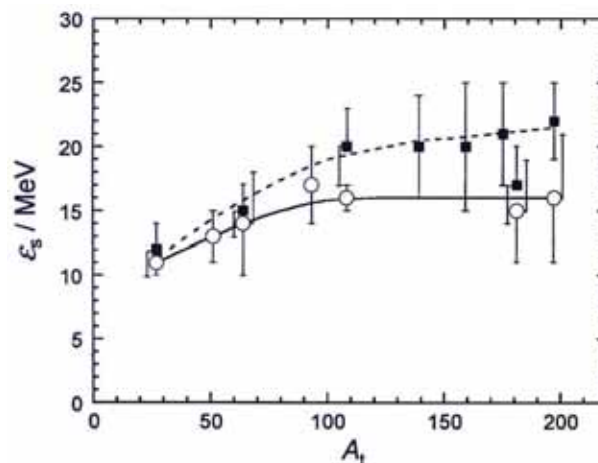


Figure 10. Parameter  $\epsilon_s$  as a function of  $A_t$  for photon reaction (open circles connected by a solid line) and proton reaction (closed squares connected by a dashed line). (From Ref. 20 with permission from the Oldenbourg Wissenschaftsverlag).

reactions was found for the first time to increase with of  $A_t$  up to  $A_t = 100$  and to become almost constant at heavier targets, showing higher values in the former compared to those in the latter. This finding is consistent with the implication of the slope difference of  $(N/Z)_p$  vs.  $(N/Z)_t$  of photo- and hadron-reactions discussed in Sec. 3.2 (Fig. 2).

Twenty nine radionuclides with  $A = 24 - 131$  produced mostly from fission of  $^{197}\text{Au}$  were identified in the target and catcher foils in addition to 20 nuclides with  $A = 152 - 197$  cited above. The effective mean ranges FW and BW were also found to be independent of  $E_0$  at the studied  $E_0$ . The F/B ratios at  $E_0 \geq 600\text{MeV}$  are plotted by open circles as a function of mass difference in Figure 11a. The F/B ratio represents the extent of forward peaking of the recoil, and thus is a

measure of the angular distribution of the product nuclei. As mentioned above, the F/B ratio from photospallations is independent of  $\Delta A$  and of  $A_t$ , and the weighted mean value for  $^{197}\text{Au}$  at  $\Delta A \leq 45$  is  $2.5 \pm 0.6$  as indicated by a dashed line in Fig. 11a. The F/B ratios at  $\Delta A \geq 66$  are also independent of  $\Delta A$ , but the weighted mean value of  $F/B = 1.1 \pm 0.1$  shown by a solid line in Fig. 11a is apparently lower than that for photospallation at  $\Delta A \leq 45$ , indicating the isotropic angular distribution of the product nuclei. The F/B ratios at  $E_p \leq 3\text{GeV}$  (open symbols) are apparently higher than those at the higher  $E_p$  (closed symbols) and also those of the photoreaction (open circles). The kinetic

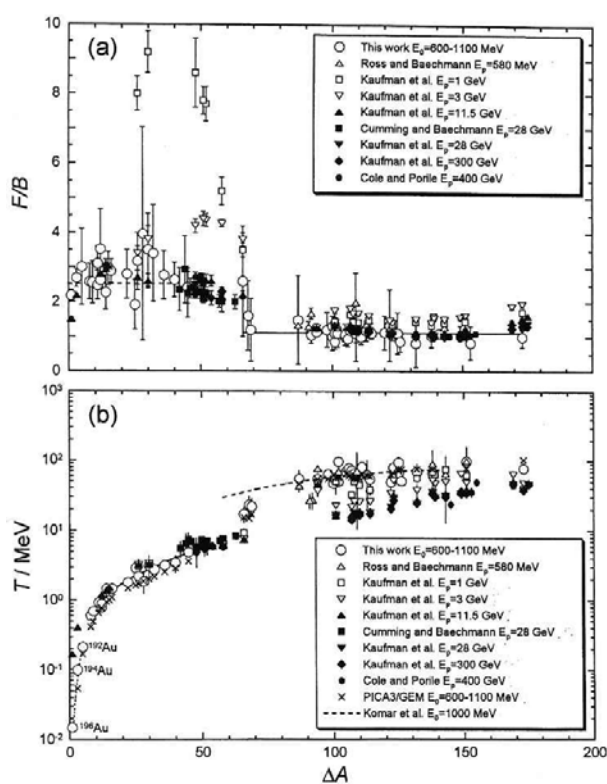


Figure 11. (a) Forward-to-backward ratios  $F/B$  and (b) kinetic energy  $T$  for  $^{197}\text{Au}$  at  $E_0 \geq 600\text{ MeV}$  as a function of  $\Delta A = (A_t - A)$ . See Refs.24 and 26 for the quoted refs. in the inset. (From Ref. 24 and 26 with permission from the Japan Society of Nucl. Radiochem. Society).

energies  $T$  of the product nuclei were evaluated by the same way as above, and are shown as a function of  $\Delta A$  for  $E_0 \geq 600\text{ MeV}$  by open circles in Fig. 11b. The  $T$  values increases with an increase of  $A$  at  $\Delta A \leq 45$ , showing the two components: one is a steep rise for the  $(\gamma, xn)$ ,  $x \geq 1$ , products as noted as  $^{196,194,192}\text{Au}$  (a dotted curve), and the other

is a gradual increase for the  $(\gamma, xnyp)$ ,  $x, y \geq 1$ , products (a solid curve). The latter component corresponds to the spallation described above. The  $T$  values at  $\Delta A > 45$  are quite high compared with those extrapolated from the spallation trend at  $\Delta A \leq 45$ . Komar et al. [75] reported the kinetic energies of coincident fragment pairs from the photofission of  $^{197}\text{Au}$  at  $E_0 = 1000\text{ MeV}$  by using the semiconductor detectors, and their results are indicated by a dashed curve in Fig. 11b which are consistent with our radiochemical ones except for those of Ba isotopes at  $\Delta A = 66, 68$  and  $69$  located in between the trends of spallation and fission. Also shown in Fig. 11b are the proton results (see the inset for data base) that change at  $\Delta A = 66$ . The  $T$  values calculated by the PICA3/GEM code are indicated by crosses in Fig. 11b at  $E_0 = 600 - 1000\text{ MeV}$  and are shown to reproduces the  $T$  values at  $\Delta A > 45$ , implying that the products are formed in the two-body breakup process, though the code underestimates a little bit for spallation region of  $\Delta A \leq 45$ .

## 6. Photopion Nuclear Reactions

### 6.1 Historical Aspects and Difficulties of Experiments

As mentioned in Introduction, the reaction yields of  $^{11}\text{B}(\gamma, \pi^-)^{11}\text{C}$ ,  $^{27}\text{Al}(\gamma, \pi^+)^{27}\text{Mg}$ ,  $^{51}\text{V}(\gamma, \pi^-xn)^{51-x}\text{Cr}$  for  $x = 0$  and  $2$ , and  $^{51}\text{V}(\gamma, \pi^+)^{51}\text{Ti}$  had been reported many times by different authors from the theoretical and experimental interests before 1970s.

A common problem in activation methods is the presence of non-mesic interactions: secondary protons and neutrons lead to the same products of  $(\gamma, \pi^-xn)$  and  $(\gamma, \pi^+)$  reactions through  $(p, x'n)$  and  $(n, p)$  reactions, respectively. This secondary contribution had been noticed in the earlier studies, but not well studied before our findings for the disentangling. In the past, the secondary neutrons were considered to be generated in the accelerators, and the contribution was estimated from off-beam samples. We examined the same procedure and also the depth profiles of the yield by using a stack of target plates, and found that these were not good for the proper correction. Then we noticed that the measurements below and above the thresholds for pion production shall be emphasized to assess the contributions of the interfering reactions. In Figure 12, the observed yields of  $^{49}\text{Cr}$  from  $^{51}\text{V}$  irradiations at  $E_0 = 30 - 1050\text{ MeV}$  are shown, as examples, to constitute smooth

curves having a step around the photopion threshold; below the step the nuclide production is purely due to the secondary reaction which is superimposed by photopion reaction above its threshold. The secondary-corrected yields increase rapidly from the threshold with an increase of  $E_0$  and attain a plateau around 300 – 500 MeV, suggesting that photon responsible for production of these nuclides are mostly of energies lower than 400 MeV. The detailed description of the correction method and its empirical expression for the secondary contributions as a function of the target mass  $A_t$  and the number of neutrons emitted  $x$  were given [7, 8, 76].

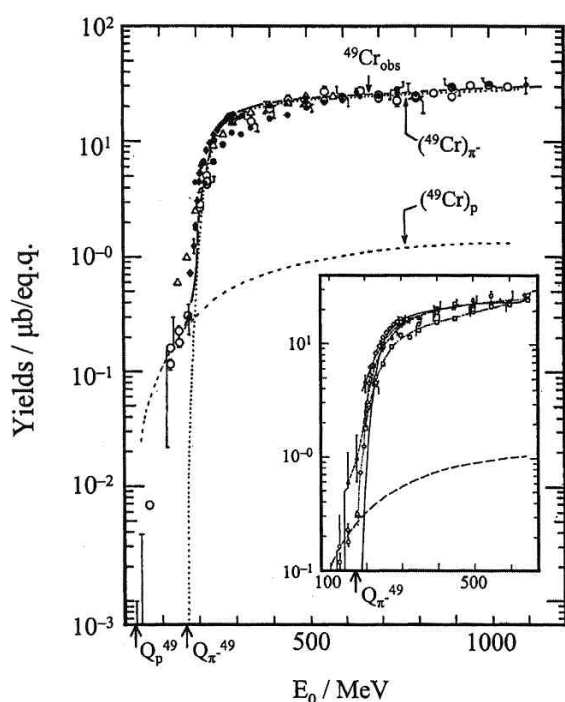


Figure 12. The  $^{49}\text{Cr}$  yields from photoreaction on  $^{51}\text{V}$  as a function of  $E_0$  for 30-1050 MeV. Open circles connected with a solid line are from our work [7]. The dashed line indicates the yields from the secondary ( $^{49}\text{Cr}$ )<sub>p</sub>. The net yields obtained from subtraction of ( $^{49}\text{Cr}$ )<sub>p</sub> from the observed yields ( $^{49}\text{Cr}$ )<sub>obs</sub> are for  $^{51}\text{V}(\gamma \pi^- 2n) ^{49}\text{Cr}$  and shown by a dotted curve noted with ( $^{49}\text{Cr}$ )<sub>π<sup>-</sup></sub>. Comparisons are made with the reported ones: closed diamonds by R. A. Meyer and J. P. Hummel, Phys. Rev., **140** (1965) B48, closed circles by G. Nydal and B. Forkman, Nucl. Phys., **B7**(1968) 97, B. Bulow et al., Z. Phys., **A278** (1976)89, and Ref. 40, and triangles from Ref.41. An inset is an expanded one in  $100 \leq E_0 \leq 650$  MeV for a detailed comparison with the literature data for ( $^{49}\text{Cr}$ )<sub>π<sup>-</sup></sub>. Arrows on  $E_0$  axis show the Q-values for  $^{41}\text{V}(p,3n)^{49}\text{Cr}$  and  $^{51}\text{V}(\gamma, \pi^- 2n)^{49}\text{Cr}$ . (Reprinted from Ref. 7 with permission from the Elsevier Ltd.).

### 6.2. Revisit to Photopion Reactions on $^{51}\text{V}$ and Findings of Reaction Yields of $^{133}\text{Cs}(\gamma, \pi^- xn) ^{133-x}\text{Ba}$ for $x$ upto 9.

The yields,  $Y(E_0)$  in unit of barn per equivalent quanta, b/eq.q., are expressed as

$$Y(E_0) = \frac{\int_0^{E_0} \sigma(k) \cdot N(E_0, k) dk}{(1/E_0) \int_0^{E_0} k \cdot N(E_0, k) dk} \quad (6)$$

a measured example of which is shown in Fig. 12 above. The yields can be unfolded into cross section  $\sigma(k)$  per photon of energy  $k$ . An example of the unfolding performed after the method of Tesh [77] with aid of the LOUHI-82 code [78] by assuming the Schiff spectrum [79] to approximate the bremsstrahlung production cross section, is shown by a thick line in Figure 13, together with the reported results (thin lines) and theoretical predictions (dotted curves). The Monte Carlo intranuclear Cascade-evaporation calculation by using the PICA code was performed, and compared also with the our result. The reported excitation curves from experiments and theoretical calculations are in disagreement with the present one, and the reasons of the discrepancies were commented in some details [7].

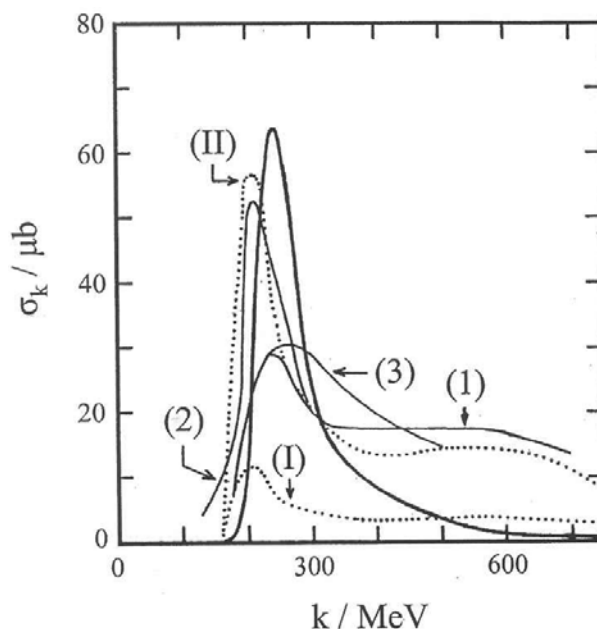


Figure 13. Comparison of the present cross section,  $\sigma_k$  (thick line) with the reported results (thin lines 1, 2 and 3) and theoretical predictions (dotted curves [ , surface production and [ [ , volume production). See Ref. 7 for the quoted references. (Reprinted from Ref. 7 with permission from the Elsevier Ltd.).

At the same time, seven Ba isotopes produced in  $^{133}\text{Cs}$  targets irradiated at  $E_0 = 30 - 1050$  MeV were found with our surprise, and the yields ascribable to the reactions of  $^{133}\text{Cs}(\gamma, \pi^-xn)$  for  $x = 0, 2, 4, 5, 6, 7$  and  $9$  showed a broad maximum at around  $x = 3$ , indicating that the excitation energy remaining after  $\pi^-$  emission is sufficiently high to evaporate  $7$  to  $9$  neutrons with appreciable probabilities, quite different from that of  $^{51}\text{V}(\gamma, \pi^-xn)$ , in which the yields decrease rapidly with an increase of  $x$  from  $0$  to  $3$ . We then unfolded the secondary-corrected yields of  $^{133}\text{Cs}(\gamma, \pi^-xn)$  reactions for  $x = 0 - 9$  into cross sections to obtain the excitation functions, the characteristics of which were extracted and discussed [8].

It was found here that the  $(\gamma, \pi^-xn)$  channel amounts only to about  $0.6\%$  of the total absorption deduced from our photospallation yields of  $^{51}\text{V}$  and/or  $^{133}\text{Cs}$ , and that the secondary interfering contributions to the photopion reactions mentioned above are not negligible.

### 6.3. Systematic Study on Characteristics of the $(\gamma, \pi^-xn)$ Yields.

We have then extended this type of experiments to other heavier and lighter targets: the measured yields for  $(\gamma, \pi^-xn)$  reactions as a function of  $x$  (isotopic mass yield distributions) exhibit a smooth function of  $A_t$  and  $E_0$ . Figure 14 shows the isotope yield distributions from  $^{51}\text{V}$ ,  $^{59}\text{Co}$ ,  $^{75}\text{As}$ ,  $^{89}\text{Y}$ ,  $^{109}\text{Ag}$ ,  $^{115}\text{In}$ ,  $^{133}\text{Cs}$ ,  $^{139}\text{La}$ ,  $^{175}\text{Lu}$ ,  $^{197}\text{Au}$  and  $^{209}\text{Bi}$  targets at  $E_0 = 800, 400$  and  $250$  MeV. At the former two  $E_0$ , the yield values are almost the same and higher than those at  $E_0 = 250$  MeV, reflecting characteristics of the  $\Delta$ -resonance. The difference between the yield patterns for  $E_0 = 250$  MeV and  $400$  (and  $800$  MeV) increases with the increasing  $A_t$ , and it becomes more prominent at larger  $x$  in the  $A_t$  region from  $127$  to  $209$ . It is clearly shown that the reactions of high neutron multiplicities become progressively more possible as  $A_t$  increases and that the reaction probabilities for  $x = 2 - 7$  and even more at  $E_0 \geq 400$  MeV are nearly comparable for heavy targets such as  $^{175}\text{Lu}$ ,  $^{197}\text{Au}$  and  $^{209}\text{Bi}$ , though not at  $E_0 = 250$  MeV. The reactions with such high neutron multiplicities are not possible for lighter targets with  $A_t \leq 100$ . The neutron multiplicity reflects primarily the excitation energy left after pion emission, while the energy spectrum of neutrons to be known. To understand the yield variations quantitatively, the widths of the mass yield curves at  $E_0 = 400$  and  $250$  MeV are

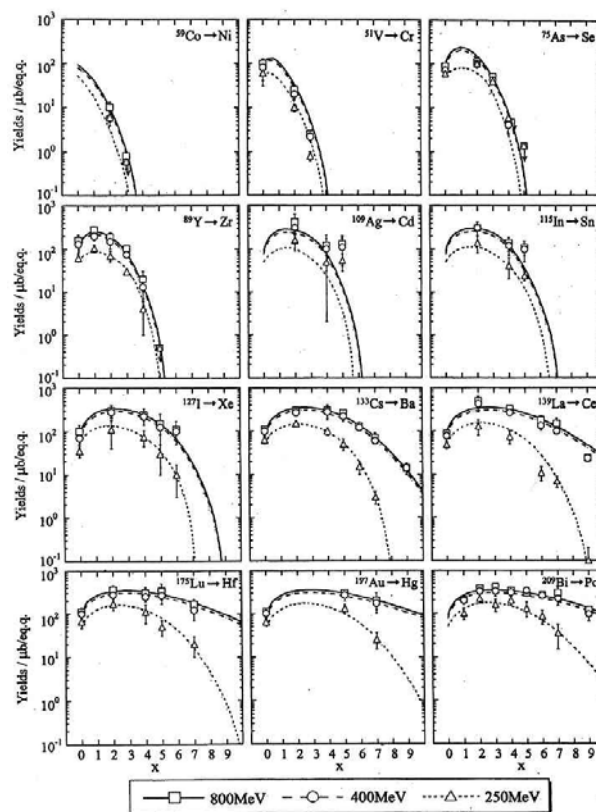


Figure 14 Variations of  $(\gamma, \pi^-xn)$  reaction yields as a function of number of emitted neutrons  $x$  at  $E_0 = 800$  MeV (squares connected by solid curves),  $400$  MeV (circles - connected by broken curves) and  $250$  MeV (triangles connected by dotted curves). (Reprinted from Ref. 10 with permission from the American Physical Society).

defined as the  $x$  values of the  $(\gamma, \pi^-xn)$  reaction, for which the yield is equal to that of the  $(\gamma, \pi^-)$  reaction,  $78 \mu\text{b}/\text{eq.q.}$  for  $E_0 = 400$  MeV and  $51 \mu\text{b}/\text{eq.q.}$  for  $E_0 = 250$  MeV (see Fig. 17 in Sec. 6.4 below) and plotted as a function of the neutron-to-proton ratio of the target,  $(N/Z)_t$  in Figure 15. The target-dependent variation of the yields is not parameterized by target mass  $A_t$  nor by the number of target neutrons  $N_t$ , because the  $(\gamma, \pi^-2n)$  and  $(\gamma, \pi^-3n)$  yields from  $^{51}\text{V}$  were found to be higher by a factor of  $3$  than those from  $^{59}\text{Co}$ , as seen in the upper left corner of Fig. 14. The degree of the increase of the width at  $E_0 = 400$  MeV is not monotonic, but changes largely at  $(N/Z)_t = 1.32 - 1.40$  ( $^{109}\text{Ag} - ^{127}\text{I}$ ), the rate of increase become smaller at  $(N/Z)_t = 1.32 - 1.35$  ( $^{109}\text{Ag} - ^{115}\text{In}$ ) and  $1.49 - 1.52$  ( $^{197}\text{Au} - ^{209}\text{Bi}$ ). The change of the width at  $E_0 = 250$  MeV is small, but the rate of increase changes also at  $(N/Z)_t = 1.35$ . The peak positions also increase with an increase of  $(N/Z)_t$  in a

manner similar to the widths. Further investigations of the yield profiles in terms of  $(N/Z)_t$  revealed that their changes at  $A_t \geq 100$  are associated with pronounced "nuclear medium effects" giving rise to more excessive excitation as compared with medium-heavy targets of  $A_t \leq 100$ . It is noted that the original PICA code overestimates the yield values of the  $(\gamma, \pi^-xn)$  reactions for  $x \geq 3$  by a factor of about 2, but the PICA-98 and PICA3/GEM reproduce them well (See Figure 16). The latter codes consider the medium effect on the N-N scattering cross section.

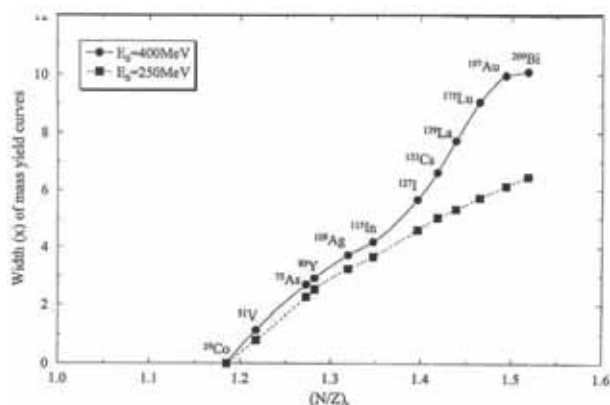


Figure 15. Widths of the isotopic mass yield curves in Fig.14, as a function of the neutron-to-proton ratio of target,  $(N/Z)_t$  at  $E_0 = 400$  and  $250$  MeV. See the text for the definition of the "width". (Reprinted from Ref. 10 with permission from the American Physical Society).

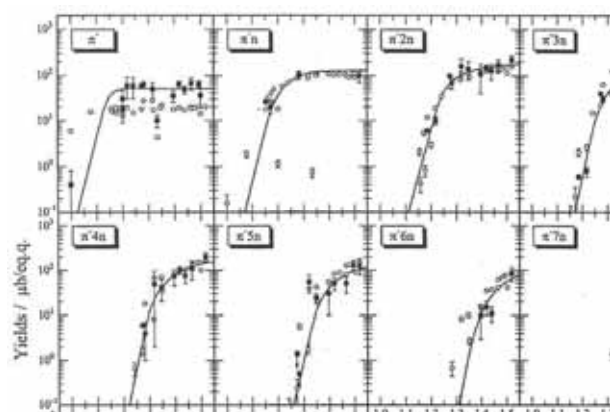


Figure 16. Variations of the  $(\gamma, \pi^-xn)$  reaction yields for  $x = 0 - 9$  as a function of the proton-to-neutron ratio of target,  $(N/Z)_t$  at  $E_0 = 400$  MeV. A comparison of PICA3/GEM calculation shown as open circles is made with the experimental values shown by closed squares. (Reprinted from Ref. 10 with permission from the American Physical Society).

#### 6.4. $A_t$ - and $E_0$ -dependence of $(\gamma, \pi^\pm)$ Yields

It is notable that the yields for  $(\gamma, \pi^-)$  reactions ( $x = 0$ ) are almost the same for all of the studied targets at  $E_0 = 800, 400$  and  $250$  MeV, as can be read at  $x = 0$  in Fig. 14. Now the yield values both for the  $(\gamma, \pi^-)$  and  $(\gamma, \pi^+)$  reactions are plotted against  $A_t$  in Figure 17 (a-c). Closed circles represent the yields for  $(\gamma, \pi^-)$  reactions on the targets indicated on the upper horizontal axis of Fig. 17(b). The large symbols show our values and

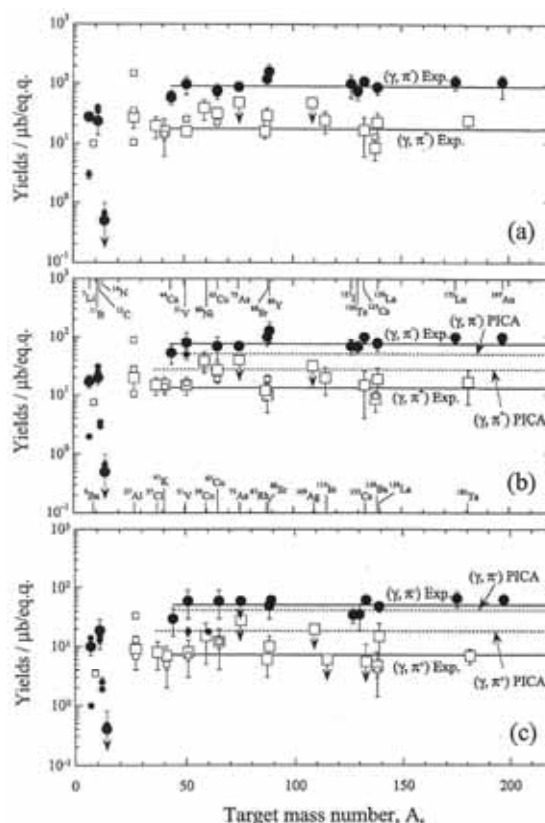


Figure 17. Target mass dependence of the  $(\gamma, \pi^\pm)$  yields at  $E_0 = 800$  MeV (a)  $E_0 = 400$  MeV, (b)  $E_0 = 250$  MeV and (c) closed circles represent the  $(\gamma, \pi^-)$  yields and open squares the  $(\gamma, \pi^+)$  yields. The large symbols show the values obtained by our group and the small ones from literature (see Ref. 7), as measured on targets indicated along the upper horizontal axis for the  $(\gamma, \pi^-)$  reactions and the lower axis for the  $(\gamma, \pi^+)$  reactions in (b). The arrow symbols show the measured yields not corrected for the secondary contributions. The solid lines are the weighted means of  $Y(E_0)$  for  $(\gamma, \pi^-)$  reactions on targets with  $A_t \geq 44$  and for  $(\gamma, \pi^+)$  reactions on  $A_t \geq 27$ . The dotted lines in (b) and (c) show the average PICA results calculated for the same reactions as with the experiments. (Reprinted from Ref. 10 with permission from the American Physical Society).

the small ones the literature data. The yield values for  $(\gamma, \pi^+)$  reactions are plotted as open squares for the targets indicated on the lower horizontal axis of Fig. 17(b). The symbols with an arrow indicate the values of upper limit, *i.e.* no corrections for the secondaries (about 10 % or less for  $^{75}\text{As}$  and  $^{109}\text{Ag}$  targets, for example, were performed. The code is only applicable to the reactions at the energy range of 30 – 400 MeV and on targets of  $A_t \geq 12$ , so the calculation at  $E_0 = 800$  MeV is not shown.

It is now clear that the yield values are  $A_t$ -independent with some exceptions of those for lighter targets where small numbers of particle stable states exist. The weighted means of the yield values of  $(\gamma, \pi^+)$  reactions on targets with  $A_t \geq 27$  are  $18 \pm 2$ ,  $14 \pm 2$  and  $7.3 \pm 1.1$   $\mu\text{b}/\text{eq.q.}$  and those of  $(\gamma, \pi^-)$  reactions for  $A_t \geq 44$  are  $91 \pm 6$ ,  $78 \pm 6$ , and  $51 \pm 5$   $\mu\text{b}/\text{eq.q.}$ , respectively at  $E_0 = 800$ , 400 and 250 MeV. The PICA calculations for the corresponding reactions at  $E_0 = 400$  and 250 MeV are also shown by dotted lines in Fig. 17(b) and (c), respectively, indicating the  $A_t$ -independences of the yields of both types of reactions. The code is only applicable to the reactions at the energy range of 30 – 400 MeV and on targets of  $A_t \geq 12$ , so the calculation at  $E_0 = 800$  MeV is not shown. The yield values are two times larger than the measured ones for  $(\gamma, \pi^+)$  reaction and 35% smaller than the measured  $(\gamma, \pi^-)$  yields. The measured yields in the  $A_t$ -independent region at  $E_0 = 400 - 800$  MeV give a yield ratio of  $Y(\gamma, \pi^-) / Y(\gamma, \pi^+) = 5.6 \pm 1$ , while the corresponding PICA value at  $E_0 = 400$  MeV is  $1.8 \pm 0.3$ .

The high observed yield ratios compared with the calculation may imply new nuclear structure effects that are not taken into consideration in theoretical ground in the PICA code. The nuclear model used in the theoretical calculation is the same as one used in the Bertinis calculation [80]. The neutron to proton density ratio in the nucleus are assumed to be equal to that of the entire nucleus. Cross sections for the photoabsorption by a nucleon in the (3,3) resonance region are taken from those for elementary processes for free nucleon- photon interactions, by assuming  $\sigma(\gamma p \rightarrow n\pi^+) = \sigma(\gamma n \rightarrow p\pi^-)$  from charge-symmetry consideration. The intranuclear cascade calculation of Bertini is then used to account for the secondary effect of nucleon- and pion-interactions with the remaining nucleus following the initial photon interaction. Pion absorption was assumed to occur via two-nucleon mechanism with a cross section

for the absorption of a charged pion by a nucleon with isobaric spin projection of the opposite sign, *i.e.* a pair of nucleons must contain at least one proton to absorb a negative pion and at least one neutron to absorb a positive pion. The higher yields of  $(\gamma, \pi^-)$  reactions and the lower ones of the  $(\gamma, \pi^+)$  reactions relative to those expected from the PICA calculation could possibly be explained if the neutron density in nuclear surface region is higher than the inner density of the nucleus. An initial production of negative pions by way of  $\gamma + n \rightarrow \Delta^0 \rightarrow p + \pi^-$  would be more probable than those of positive pions by way of  $\gamma + p \rightarrow \Delta^+ \rightarrow n + \pi^+$ , and the secondary absorption of negative pion by way of  $\pi^- + pp$  or  $\pi^- + pn$  would be less than those of positive pions by way of  $\pi^+ + np$  or  $\pi^+ + nn$  in the neutron-rich surface region.

These processes that lead to  $(\gamma, \pi^-)$  and  $(\gamma, \pi^+)$  reactions are, therefore, considered to occur in the surface region of the nucleus, but the cross sections and/or the yields are not proportional to  $A_t^{2/3}$  but  $A_t$ -independent. This  $A_t$ -independence may be explained as due to compensation of the increase in pion production with increasing nuclear size (surface) by the competitive increase of neutron emissivity associated with pion emission as seen in Sec. 6.3 above in the characteristic features of the  $(\gamma, \pi^-xn)$  yields. There has been no observation of the density difference between neutrons and protons in the stable nucleus, but the neutron skin and neutron halo structures have been discovered in very neutron-rich nuclei near the drip line. Further study of structural changes in nuclei closer to the  $\beta$ -stability line is required. Our work suggests that photonuclear processes may cause such effects.

## 7. Summary and Perspectives

1. All aspects of the final product nuclei from photonuclear reactions, *i.e.* spallation, fragmentation, fission and photopion reaction, induced by bremsstrahlung of the end point energies of  $E_0 = 30 - 1200$  MeV have been investigated systematically with respect to photon energy  $k$  and/or  $E_0$ , target masses  $A_t$ , product masses  $A$  and their compositions. Irradiations have been performed in small steps of  $E_0$  of 100 MeV or less to be able to unfold the yields into cross sections as a function of photon energy  $k$ . A simple nuclear recoil experiment using thick-target thick-catcher method was performed on 167 radionuclides formed from

seven targets of  $^{27}\text{Al} - ^{197}\text{Au}$  to obtain kinematic information.

2. Photospallation has been systematized in terms of MD and CD, and the parameters of the empirical equations have been revised. The difference of the characteristics of photo- and hadron-spallations has been clarified. The photon-induced intranuclear cascade and evaporation analysis (PICA) code by Gabriel and Alsmiller and its revised versions have been tested by our new data.
3. The light nuclear fragments, such as  $^{7,10}\text{Be}$  and  $^{22,24}\text{Na}$ , as well as other light- and medium-weight radionuclides extending to spallation and/or fission product regions formed from 23 targets ranging from  $^{\text{nat}}\text{B}$  to  $^{197}\text{Au}$  at  $E_0 = 250 - 1200$  MeV in steps of 100 MeV or less have been measured radiochemically. For the  $^{10}\text{Be}$  measurement, AMS technique was applied. The  $A_T$ -dependent variations of the  $^{7,10}\text{Be}$ ,  $^{22,24}\text{Na}$  and  $^{28}\text{Mg}$  yields were found for the first time to have two components, due to spallation and fragmentation. It was also found that the fragment formation is largely dependent on target properties: the neutron-rich fragments are more probable from heavier targets with higher  $(N/Z)_t$ .
4. Photofission of  $^{197}\text{Au}$  and  $^{209}\text{Bi}$  was investigated by measuring radiochemically 58 products in a mass range of  $A = 42 - 131$  at  $E_0 = 300 - 1000$  MeV and 63 products in a mass range of  $A = 56 - 136$  at  $E_0 = 450 - 1000$  MeV, respectively, in  $E_0$  steps of 50 - 100 MeV with use of the catcher foil technique. The characteristics of the CD, MD, the recoil properties and also the total fission yields were investigated by referring to the PICA3/GEM calculation. A comparison was made for the present results with the reported proton fissions.
5. Photopion reactions of  $(\gamma, \pi^\pm)$  and  $(\gamma, \pi^\mp xn)$  types were radiochemically studied on 27 targets of  $^7\text{Li}$  to  $^{209}\text{Bi}$  at  $E_0 = 30 - 1050$  MeV in steps of 50 MeV or less. Starting with a revisit to one of the most studied reactions,  $^{51}\text{V}(\gamma, \pi^\pm)$  and  $^{51}\text{V}(\gamma, \pi^\mp xn)$  for  $x$  up to 3, a new correction method for the interfering secondary particle induced reactions was devised, and the secondary-corrected yield curves were successfully unfolded into cross sections per photon of monochromatic energy  $k$ . Comparison with the literature data showed the discrepancies from our results both on the yield curves and

excitation functions. Theoretical calculations based on a valence nucleon model, an impulse approximation with and without final state interaction of the outgoing pion and a combination of valence and volume production model were found to be not in agreement with our excitation functions. We have then extended our measurements to the mentioned wide region of targets, and found that the yields of the  $(\gamma, \pi^\mp xn)$  reactions up to  $x = 9$  are smooth functions of  $x$ , target composition of  $(N/Z)_t$  and exhibit a pronounced nuclear medium effects for  $(N/Z)_t \geq 1.3 - 1.4$ , *i.e.*  $A_t \geq 110 - 130$ . This has proved by an excellent reproduction by the calculations with use of the revised code of PICA, PICA3/GEM by Sato et al. The  $(\gamma, \pi^\pm)$  yields from medium and heavy targets were found to be  $A_T$ -independent, irrespective of  $E_0$ . The yield ratios of  $Y(\gamma, \pi^-) / Y(\gamma, \pi^+)$  are 5 - 6, whereas the PICA code gives the ratio of 2. The discrepancy seems to be explained if the neutron density in nuclear surface region is higher than the inner density of the nucleus. This channel is found to be very informative of reaction mechanism, though the cross sections are small.

6. Perspectives. It is worth of mentioning that the theoretical treatment in the framework of  $\Delta$ -hole model by Koch et al. [81] would be applied to the further interpretations of the present results. The type of our experiments has to be extended to GeV region, where the shadowing effect would manifest itself. The interaction of the incident photons with the target nucleus is reported to start to resemble a hadronic process above the  $\Delta$ -resonance region; the incident photons mainly interact with surface nucleons leaving the interior of the nuclear volume "shadowed". The shadowing effects are included in PICA3/GEM. This effect is an issue of current interest. Furthermore, very interesting is that an application of our study on  $(\gamma, \pi^\mp xn)$  reactions,  $x = 0 - 9$ , to elucidate nuclear charge pickup ( $\Delta Z = +1$ ) of the projectiles at ultra-relativistic heavy-ion (158A GeV Pb) collisions has recently been pointed out [82, 83].

The Large Hadron Collider (LHC) at CERN and the Relativistic Heavy Ion Collider (RHIC) at BNL aim the study of a possible phase transition of nuclear and hadronic matter into the quark-gluon plasma at high energy densities, the conditions of which are believed to have existed in the early

universe soon after the big bang. The general picture of ultra-relativistic heavy-ion collision requires the investigations not only of the participant zones but also of peripheral collisions where the electromagnetic interactions are considered to play important roles.

### Acknowledgement

The works accounted in this article have been performed during the period when the author was at the Department of Chemistry of Kanazawa University by collaborations of the author's students totaling more than one half of 150 who finished their BS, MS and D.Sc. thesis on the parts of the present work. Professor S. Shibata of Kyoto University, Professor Emeritus I. Fujiwara of Ottemon-Gakuin University and Professor Emeritus M. Furukawa are deeply thanked for their pleasant collaborations in the works and for their kind guidance to the students since the earlier stage of the series of the experiments. Also thanked are the staff and crew members of the KEK ES, the ETL ES and the LNS Linac for their cooperations in accelerator operations. The author appreciates the permissions to use the published materials from the copyrighters: the Elsevier Ltd., the American Physical Society, the Oldenbourg Wissenschaftsverlag and the Japan Society of Nuclear and Radiochemical Sciences.

### References

- [1] H. Arenhövel and D. Drechsel, ed. Nuclear Physics with Electromagnetic Interactions Proc. Int. Conf. on Nuclear Physics with Electromagnetic Interactions, Mainz, 1979, Vol. 108 of Lecture Notes in Physics (Springer-Verlag, Berlin, 1979)
- [2] P. Stoler, ed. Photopion Nuclear Physics, (Plenum, New York, 1979)
- [3] A. Nagl, V. Devanathan and H. Überall, Nuclear Pion Photoproduction (Springer-Verlag, Berlin, 1991)
- [4] I.S. Hughes and P.V. March, Proc. Phys. Soc. (London) **72** (1958) 259.
- [5] K. Sakamoto, J. Nucl. Radiochem. Soc. **4** (2003) A9.
- [6] G. G. Jonsson and B. Persson, Nucl. Phys. **A153** (1970) 32.
- [7] K. Sakamoto, M. Yoshida, Y. Kubota, T. Fukasawa, A. Kunugise, Y. Hamajima, S. Shibata and I. Fujiwara, Nucl. Phys. **A501** (1989) 693.
- [8] K. Sakamoto, Y. Hamajima, M. Soto, Y. Kubota, M. Yoshida, A. Kunugise, M. Masatani, S. Shibata, M. Imamura, M. Furukawa and I. Fujiwara, Phys. Rev. **C42** (1990) 1545.
- [9] Y. Oura, A. Yazawa, M. Yoshida, S. R. Sarkar, K. Sakamoto, S. Shibata, I. Fujiwara, and M. Furukawa, Radiochim. Acta **68** (1995) 27.
- [10] K. Sakamoto, S. R. Sarkar, Y. Oura, H. Haba, H. Matsumura, Y. Miyamoto, S. Shibata, M. Furukawa and I. Fujiwara, Phys. Rev. **C59** (1999) 1497.
- [11] K. Sakamoto, H. Toramoto, Y. Hamajima, K. Okada and M. Dohniwa, Radiochim. Acta **37** (1984) 69.
- [12] K. Sakamoto, M. Nishio, M. Dohniwa, K. Okada and Y. Hamajima, Radiochim. Acta **37** (1984) 83.
- [13] S. Shibata, M. Imamura, T. Miyachi, M. Mutou, K. Sakamoto, Y. Hamajima, M. Soto, K. Kubota, M. Yoshida and I. Fujiwara, Phys. Rev. **C35** (1987) 254.
- [14] S. R. Sarkar, M. Soto, Y. Kubota, M. Yoshida, T. Fukasawa, K. Matsumoto, K. Kawaguchi, K. Sakamoto, S. Shibata, M. Furukawa and I. Fujiwara, Radiochim. Acta **55** (1991) 113.
- [15] S. R. Sarkar, Y. Kubota, T. Fukasawa, K. Kawaguchi, K. Sakamoto, S. Shibata and I. Fujiwara, Radiochim. Acta **55** (1991) 139.
- [16] S. R. Sarkar, Y. Oura, K. Kawaguchi, A. Yazawa, K. Sakamoto, S. Shibata and I. Fujiwara, Radiochim. Acta **62** (1993) 7.
- [17] H. Haba, H. Matsumura, Y. Miyamoto, K. Sakamoto, Y. Oura, S. Shibata, M. Furukawa and I. Fujiwara, J. Radioanal. Nucl. Chem. **239** (1999) 133.
- [18] I. Fujiwara, H. Haba, H. Matsumura, K. Sakamoto, Y. Miyamoto, Y. Oura, S. Shibata and M. Furukawa, Czech. J. Phys. **49** Suppl. S1, (1999) 831.

- [19] H. Haba, H. Matsumura, K. Sakamoto, Y. Oura, S. Shibata, M. Furukawa and I. Fujiwara, *Radiochim. Acta* **85** (1999) 1.
- [20] H. Haba, H. Matsumura, K. Sakamoto, Y. Oura, S. Shibata, M. Furukawa and I. Fujiwara, *Radiochim. Acta* **88** (2000) 375.
- [21] S. Shibata, M. Imamura, K. Sakamoto, S. Okizaki, S. Shibutani, H. Matsumura, M. Furukawa, I. Fujiwara, H. Nagai and K. Kobayashi, *Radiochim. Acta* **80** (1998) 181.
- [22] H. Matsumura, K. Washiyama, H. Haba, Y. Miyamoto, Y. Oura, K. Sakamoto, S. Shibata, M. Furukawa, I. Fujiwara, H. Nagai, T. Kobayashi and K. Kobayashi, *Radiochim. Acta* **88** (2000) 313.
- [23] H. Haba, M. Igarashi, K. Washiyama, H. Matsumura, M. Yamashita, K. Sakamoto, Y. Oura, S. Shibata, M. Furukawa and I. Fujiwara, *J. Nucl. Radiochem. Sci.* **1** (2000) 53.
- [24] H. Haba, M. Igarashi, K. Washiyama, H. Matsumura, M. Yamashita, K. Sakamoto, Y. Oura, S. Shibata, M. Furukawa and I. Fujiwara, *J. Nucl. Radiochem. Sci.* **1** (2000) 69.
- [25] H. Haba, M. Kasaoka, M. Igarashi, K. Washiyama, H. Matsumura, Y. Oura, S. Shibata, K. Sakamoto, M. Furukawa and I. Fujiwara, *Radiochim. Acta* **90** (2002) 371.
- [26] H. Haba, *J. Nucl. Radiochem. Sci.* **3** (2002) A11.
- [27] T. A. Gabriel and R. G. Alsmiller, Jr., *Phys. Rev.* **182** (1969) 1035.
- [28] T. A. Gabriel, M. P. Guthrie and O. W. Hermann, Oak Ridge National Laboratory Report No. ORNL-4687 (1971).
- [29] C.Y. Fu, PICA 95, An Intra-Nuclear Cascade Code for 25 MeV to 3.5 GeV Photon-Induced Nuclear Reactions, presented at SATIF-3, Sendai, May 12-13, 1997.
- [30] T. Sato, K. Shin, S. Ban, Y. Namio, H. Nakamura and H. Hirayama, *Nucl. Instrum. Methods* **A437** (1999) 471.
- [31] T. Sato, K. Shin, S. Ban, T. A. Gabriel, C. Y. Fu and H. S. Lee, Proc. Advanced Monte Carlo on Radiation Physics, Particle Transport Simulation and Applications, Lisbon, Oct. 23-26, 2000 (private communication).
- [32] S. G. Mashnik, M. I. Baznat, K. K. Gudima, A. J. Sierk and R. E. Prael, *J. Nucl. Radiochem. Sci.* **6** (2005) A1.
- [33] K. Osada, T. Fukasawa, K. Kobayashi, Y. Hamajima, K. Sakamoto, S. Shibata and I. Fujiwara, Research Report of Laboratory of Nuclear Science, Tohoku University **20** (1987) 299.
- [34] R. Serber, *Phys. Rev.* **72** (1947) 1114.
- [35] G. Rudstam, *Z. Naturforsch.* **21a** (1966) 1027.
- [36] G. G. Jonsson and K. Lindgren, *Phys. Scripta* **7** (1973) 49.
- [37] G. G. Jonsson and K. Lindgren, *Phys. Scripta* **15** (1977) 308.
- [38] N. Metropolis, R. Bivins, M. Storm, J. M. Miller, G. Friedlander and A. Turkevich, *Phys. Rev.* **110** (1958) 204.
- [39] G. Rudstam, *Nucl. Phys.* **A126** (1969) 401.
- [40] B. Bülow, B. Johnsson, M. Nilsson and B. Forkman, *Z. Phys.* **A278** (1976) 89.
- [41] I. Blomqvist, P. Janeček, G. G. Jonsson, R. Petersson, H. Dinter and K. Tesch, *Z. Phys.* **A278** (1976) 83.
- [42] K. Lindgren and G. G. Jonsson, *Nucl. Phys.* **A197** (1972) 71.
- [43] V. S. Barashenkov, F. G. Geregghi, A. S. Iljinov, G. G. Jonsson and V. D. Toneev, *Nucl. Phys.* **A231** (1974) 462.
- [44] J. B. Cumming, P. E. Haustein, R. W. Stoenner, L. Mausner and R. A. Naumann, *Phys. Rev.* **C10** (1974) 739.
- [45] J. B. Cumming, R. W. Stoenner and P. E. Haustein, *Phys. Rev.* **C14** (1976) 1554.
- [46] J. B. Cumming, P. E. Haustein, T. J. Ruth and G. J. Virts, *Phys. Rev.* **C17** (1978) 1632.
- [47] M. Yamashita, K. Yoshida, Y. Terada, A. Nagano, Y. Kawashima, D. Osada, H. Matsumura, K. Washiyama, K. Sakamoto, Y. Miyamoto, Y. Oura, S. Shibata, I. Fujiwara and M. Furukawa, Proc. 43rd Symp. on Radiochemistry, Oct. 13-15, Tsukuba, Japan, Suppl. to *J. Nucl. Radiochem. Sci.*, Vol. 1(1999) Abstract 3P17.

- [48] H. Matsumura, M. Yamashita, H. Haba, Y. Terada, K. Washiyama, H. Kikunaga, Y. Oura, Y. Miyamoto, K. Sakamoto, I. Fujiwara, S. Shibata and M. Furukawa, Proc. 44th Symp. on Radiochemistry, Sep. 12-14 (2000), Kobe, Japan, Suppl. 2 to J. Nucl. Radiochem. Sci. Vol. 1(2000) Abstract 3P12.
- [49] H. Matsumura, M. Yamashita, H. Kikunaga, H. Haba, K. Washiyama, Y. Miyamoto, Y. Oura, K. Sakamoto, S. Shibata, M. Furukawa, and I. Furukawa, Proc. 2001 APSORC and 45th Symp. on Radiochemistry, Oct. 30-Nov. 1, 2001, Fukuoka, Japan. Suppl. to J. Nucl. Radiochem. Sci., Vol. 2(2001) Abstract 2P02.
- [50] J. M. Miller and J. Hudis, Ann. Rev. Nucl. Sci. **9** (1959) 159.
- [51] K. Beg and N. T. Poril, Phys. Rev. **C3** (1971) 1631.
- [52] S. M. Qaim, Radiochim. Acta **70/71** (1995) 163.
- [53] X. Campi, J. Desbois and E. Lipparini, Phys. Lett. **138B** (1984) 353.
- [54] J. Hüfner, Phys. Rep. **125** (1985) 129.
- [55] S. Shibata, M. Imamura, H. Nagai, K. Kobayashi, K. Sakamoto, M. Furukawa and I. Fujiwara, Phys. Rev. **C48** (1993) 2617.
- [56] K. Komura, Proc. 1997 Int. Symp. on Environmental Radiation, Tsuruga, Fukui, Japan (1997), ed. by T. Tsujimoto and Y. Ogawa, Kansai Branch, Atomic Energy Soc. Japan, pp.56 (Kansai Kosaido Co. Ltd. Osaka, 1998)
- [57] V. di Napoli, F. Salvetti, M. L. Terranova, H. G. de Carvalho, J. B. Martins and O. A. P. Tavares, J. Inorg. Nucl. Chem. **40** (1978) 175.
- [58] V. di Napoli, G. Rosa, F. Salvetti, M. L. Terranova, H. G. de Carvalho, J. B. Martins and O. A. P. Tavares, J. Inorg. Nucl. Chem. **37** (1975) 1101.
- [59] V. di Napoli, J. B. Martins, G. Rosa, F. Salvetti, O. A. P. Tavares, M. L. Terranova and H. G. de Carvallho, J. Inorg. Nucl. Chem. **40** (1978) 1619.
- [60] A. Järund, B. Friberg and B. Forkman, Z. Phys. **262** (1973) 15.
- [61] A. Järund and B. Forkman, Z. Phys. **281** (1977) 39.
- [62] H. Matsumura, J. Nucl. Radiochem. Sci. **16** (2006) 9.
- [63] H. J. Rose and G. A. Jones, Nature **307** (1984) 245.
- [64] E. Hourany, Carbon Decay and Fine Structure; R. Bonetti and A. Guglielmetti, Experiments on Heavy Cluster (O, F, Ne, Mg, Si) Radioactivities; D. N. Poenaru and W. Greiner, Theories of Cluster Radioactivities; R. Blendowske, T. Fließbach and H. Walliser, Many-body Approach to Alpha and Cluster Radioactivity, in Nuclear Decay Modes, ed. By D. N. Poenaru ( Institute of Physics Publishing, Bristol and Philadelphia, 1996).
- [65] R. Bonetti, A. Guglielmetti, D. N. Poenaru, W. Greiner, R. K. Gupta, M. Mirea, W. Scheid, A. Sandulescu, F. Carstoiu, S. Misicu, A. Florescu, I. Bulboaca, A. V. Ramayya, J. H. Hamilton, J. K. Hwang and G. M. Ter-Akopian, New Cluster Radioactivity and the Superasymmetric Fission; Experiments and Theory, in Heavy Elements and Related New Phenomena, ed. By W. Greiner and R. K. Gupta, (World Sci. Pub. Co., Singapore, 1999).
- [66] A. Komar, B. A. Bochagov, A. A. Kotov, Yu. N. Ranyuk, G. G. Semenchuk, G. E. Solyakin and P. V. Sorokin, Sov. J. Nucl. Phys. **10** (1970) 30.
- [67] B. Schröder, G. Nydal and B. Forkman, Nucl. Phys. **A143** (1970) 449.
- [68] V. di Napoli, A. M. Laceranza, D. Margadonna, F. Salvetti, S. M. Terenzi, H. G. de Carvalho and J. B. Martins, Gazz. Chim., Ital. **101** (1971) 117.
- [69] M. Areskoug, B. Schröder, K. Lindgren, G. Andersson and B. Forkman, Nucl. Phys. **A226** (1974) 93.
- [70] M. Areskoug, B. Schröder and K. Lindgren, Nucl. Phys. **A251** (1975) 418.
- [71] V. Emma, S. Lo Nigro and C. Milone, Nucl. Phys. **A257** (1976) 438.
- [72] L. Winsberg, Nucl. Instr. Methods **150** (1978) 465.

- [73] J. F. Ziegler, J. P. Biersack and U. Littmark, *The Stopping and Range of Ions in Solid* (Pergamon, New York, 1985).
- [74] L. Winsberg, *Phys. Rev.* **C22** (1980) 2116 and **C22** (1980) 2123.
- [75] A. P. Komar, B. A. Bochagov, A. A. Kotov, Yu. N. Ranyuk, G. G. Semenchuk, G. E. Solyakin and P. V. Sorokin, *Sov. J. Nucl. Phys.* **10** (1970) 30.
- [76] Y. Oura, *Dr. Sci. Dissertation, Kanazawa University* ( in Japanese, 1995).
- [77] K. Tesch, *Nucl. Instrum. Methods* **95** (1971) 245.
- [78] J. T. Routti and J. V. Sandberg, *Comp. Phys. Comm.* **21** (1989) 119.
- [79] L. I. Schiff, *Phys. Rev.* **83** (1951) 252.
- [80] H. W. Bertini, *Phys. Rev.* **131** (1963) 1801.
- [81] J. H. Koch, E. J. Moniz and Ohtsuka, *Ann. Phys. (N.Y.)* **154** (1984) 99.
- [82] K. A. Chikin, V. L. Korotkin, A. P. Kryukov, L. I. Sarycheva, I. A. Pshenichnov, J. P. Bondorf and I. N. Mishstin, *Eur. Phys. J.* **A8** (2000) 537.
- [83] C. Scheidenberger, I. A. Pshenichnov, T. Aumann, S. Datz, K. Sümmerer, J. P. Bondorf, D. Boutin, H. Geissel, P. Grafström, H. Knudsen, H. F. Krause, B. Lommel, S. P. Møller, G. Münzenberg, R. H. Schuch, E. Uggerhøj, U. Uggerhøj, C. R. Vane, A. Ventura, Z. Z. Vilakazi and H. Weick, *Phys. Rev. Lett.* **88** (2002) 042301.